Semiannual Technical Report

Low Temperature Deposition and Characterization of N- and P-Type Silicon Carbide Thin Films and Associated Ohmic and Schottky Contacts

Supported under Grant #N00014-92-J-1500
Office of the Chief of Naval Research
Report for the period 7/1/93–12/31/93

R. F. Davis and R. J. Nemanich*
M. C. Benjamin*, S. Kern, S. King, L. M. Porter, and S. Tanaka
Materials Science and Engineering Department
*Department of Physics
North Carolina State University
Raleigh, NC 27695

December, 1993

REPORT DOCUMENTATION PAGE

Form Approved
OMB No. 0704-0188

1. AGENCY USE ONLY (Leave blank)	2. REPORT DATE	3. REPORT TYPE AND DATES COVERED
	December, 1993	Semiannual Technical 7/1/93–12/31/93

4. TITLE AND SUBTITLE
Low Temperature Deposition and Characterization of N- and P-Type Silicon Carbide Thin Films and Associated Ohmic and Schottky Contacts

5. FUNDING NUMBERS
sic0002---02
1261
N00179
N66005
4B855

6. AUTHOR(S)
Robert F. Davis and Robert J. Nemanich

7. PERFORMING ORGANIZATION NAME(S) AND ADDRESS(ES)
North Carolina State University
Hillsborough Street
Raleigh, NC 27695

8. PERFORMING ORGANIZATION REPORT NUMBER
N00014-92-J-1500

9. SPONSORING/MONITORING AGENCY NAMES(S) AND ADDRESS(ES)
Sponsoring: ONR, Code 1261, 800 N. Quincy, Arlington, VA 22217-5660
Monitoring: Office of Naval Research Resider
The Ohio State University Research Center
1960 Kenny Road
Columbus, OH 43210-1063

10. SPONSORING/MONITORING AGENCY REPORT NUMBER

11. SUPPLEMENTARY NOTES

12a. DISTRIBUTION/AVAILABILITY STATEMENT
Approved for Public Release; Distribution Unlimited

12b. DISTRIBUTION CODE

13. ABSTRACT (Maximum 200 words)

The cleaning and etching of the vicinal α(6H)-SiC(0001) surface has been emphasized in this reporting period because of its recently demonstrated importance in the MBE of SiC and AlN films on SiC wafers and layers. Etching with a solution of 1:1:10 HF:H_2:ethanol and a hydrogen plasma sharply reduced both the oxide and the C surface concentrations as determined by AES and XPS spectra. Controlled growth of both β-SiC and α(6H)-SiC films have been achieved on SiC wafers and films. Flow ratios of C_2H_4 and Si_2H_6 of 1:1 result in 6H-SiC while C-rich ratios give 3C-SiC. Surface reconstruction as a function of surface treatment have also been related to the deposited SiC polytype. The initial stages of AlN film growth has also been investigated in terms of defects via TEM. Two types of defects were found in the AlN film: one caused by lattice mismatch; the other by the presence of steps in the SiC surface. The interfacial chemistry and microstructure, electrical properties and the Schottky barrier heights of It thin films on α(6H)-SiC(0001) surfaces were investigated after annealing to 700°C and a maximum time of 60 min. The reaction zone contained Ti_5Si_3 and TiC. The electrical properties changed little as a function of heat treatment.

14. SUBJECT TERMS
α(6H)-SiC, β-SiC, aluminum nitride, thin films, plasma etching, surface reconstruction, defects, Schottky contacts, molecular beam epitaxy, X-ray photoelectron spectroscopy, Auger spectroscopy, transmission electron microscopy

15. NUMBER OF PAGES
47

16. PRICE CODE

17. SECURITY CLASSIFICATION OF REPORT	18. SECURITY CLASSIFICATION OF THIS PAGE	19. SECURITY CLASSIFICATION OF ABSTRACT	20. LIMITATION OF ABSTRACT
UNCLAS	UNCLAS	UNCLAS	SAR

Table of Contents

I. Introduction

Silicon carbide (SiC) is a wide bandgap material that exhibits polytypism, a one-dimensional polymorphism arising from the various possible stacking sequences of the silicon and carbon layers. The lone cubic polytype, β-SiC, crystallizes in the zincblende structure and is commonly referred to as 3C-SiC. In addition, there are also approximately 250 other rhombohedral and hexagonal polytypes [1] that are all classed under the heading of α-SiC. The most common of the α-SiC polytypes is 6H-SiC, where the 6 refers to the number of Si/C bilayers along the closest packed direction in the unit cell and the H indicates that the crystal structure is hexagonal.

Beta (3C)-SiC is of considerable interest for electronic applications that utilize its attractive physical and electronic properties such as wide bandgap (2.2 eV at 300K) [2], high breakdown electric field (2.5×10^6 V/cm) [3], high thermal conductivity (3.9 W/cm °C) [4], high melting point (3103K at 30 atm) [5], high saturated drift velocity (2×10^7 m/s) [6], and small dielectric constant (9.7) [7]. Primarily due to its higher electron mobility than that of the hexagonal polytypes, such as 6H-SiC [8], β-SiC remains preferable to hexagonal SiC for most device applications.

Most 3C-SiC thin film growth to date has been performed on Si substrates. Large-area, crack-free, and relatively thick (up to 30 μm) epitaxial 3C-SiC thin films have been grown on Si (100) by exposing the Si substrate to a C-bearing gaseous species prior to further SiC growth [7, 9, 10]. However, these films exhibited large numbers of line and planar defects due to large lattice and thermal mismatches between SiC and Si. One particular type of planar defect, the inversion domain boundary (IDB), was eliminated with the use of Si (100) substrates cut 2°–4° toward [011] [11–13]. Growth on Si substrates has allowed much understanding of SiC growth processes and device development to occur, but the large thermal and lattice mismatches between SiC and Si hamper further development using Si substrates. As a result, great effort has been made to develop methods for growth SiC single crystal substrates for homoepitaxial growth of SiC thin films.

Since the 1950's, monocrystalline single crystals of 6H-SiC have been grown at using the Lely sublimation process [14]. However, nucleation was uncontrolled using this process and control of resultant polytypes was difficult. SiC single crystals inadvertently formed during the industrial Acheson process have also been used as substrates for SiC growth. However, neither these crystals or those formed using the Lely process are large enough for practical device applications. Recently, using a seeded sublimation-growth process, boules of single polytype 6H-SiC of > 1 inch diameter of much higher quality of that obtained using the Lely process have been grown. The use of single crystals of the 6H polytype cut from these boules has given a significant boost to SiC device development.

Silicon carbide epitaxial thin film growth on hexagonal SiC substrates has been reported since the 1960's. The use of nominally on-axis SiC substrates has usually resulted in growth of 3C-SiC films. Films of 3C-SiC (111) grown by CVD have been formed on 6H-SiC substrates less than 1° off (0001) [15]. Films of 3C-SiC on 6H-SiC substrates have typically had much lower defect densities than those grown on Si substrates. The major defects present in 3C-SiC/6H-SiC films have been double positioning boundaries (DPB) [16]. Despite the presence of DPBs, the resultant material was of sufficient quality to further device development of SiC. The use of off-axis 6H-SiC (0001) substrates has resulted in growth of high-quality monocrystalline 6H-SiC layers with very low defect densities [17].

In addition, the use of more advanced deposition techniques, such as molecular beam epitaxy (MBE), has been reported for SiC in order to reduce the growth temperature and from about 1400–1500°C on 6H-SiC substrates. Si and C electron-beam sources have been used to epitaxially deposit SiC on 6H-SiC (0001) at temperatures of 1150°C [18]. Ion-beam deposition of epitaxial 3C-SiC on 6H-SiC has also been obtained at the temperature of 750°C using mass-separated ion beams of $^{30}Si^{+}$ and $^{13}C^{+}$ [19].

Aluminum nitride (AlN) is also of particular interest at this time because of its very large bandgap. It is the only intermediate phase in the Al-N system and normally forms in the wurtzite (2H-AlN) structure. Most current uses of AlN center on its mechanical properties, such as high hardness (9 on Mohs scale), chemical stability, and decomposition temperature of about 2000°C [20]. Properties such as high electrical resistivity (typically $\geq 10^{13}$ Ω-cm), high thermal conductivity (3.2 W/cm K) [21], and low dielectric constant ($\varepsilon \approx 9.0$) make it useful as a potential substrate material for semiconductor devices as well as for heat sinks. The wurtzite form has a bandgap of 6.28 eV [22] and is a direct transition, thus it is of great interest for optoelectronic applications in the ultraviolet region.

Because of the difference in bandgaps (2.28 eV for 3C-SiC and 6.28 eV for 2H-AlN) between the materials, a considerable range of wide bandgap materials, made with these materials, should be possible. Two procedures for bandgap engineering are solid solutions and multilayers. A particularly important factor is that the two materials have a lattice mismatch of less than one percent.

Research in ceramic systems suggests that complete solid solubility of AlN in SiC may exist [23]. Solid solutions of the wurtzite crystal structure should have E_g from 3.33 eV to 6.28 eV at 0 K. Although it has not been measured, the bandgap of cubic AlN has been estimated to be around 5.11 eV at absolute zero and is believed to be indirect [24]. Cubic solid solutions should thus have E_g from 2.28 eV to roughly 5.11 eV at 0 K and would be indirect at all compositions if theory holds true.

Because of their similarity in structure and close lattice and thermal match, AlN-SiC heterostructures are feasible for electronic and optoelectronic devices in the blue and infrared

region. Monocrystalline AlN layers have been formed by CVD on SiC substrates [25] and SiC layers have been formed on AlN substrates formed by AlN sputtering on single crystal W [26]. In addition, theory on electronic structure and bonding at SiC/AlN interfaces [24] exists and critical layer thicknesses for misfit dislocation formation have been calculated for cubic AlN/SiC [27]. Note that AlN (at least in the wurtzite structure) is a direct-gap material and SiC is an indirect gap material. Superlattices of these materials would have a different band structure than either constituent element. The Brillouin zone of a superlattice in the direction normal to the interfaces is reduced in size. This reduction in zone size relative to bulk semiconductors causes the superlattice bands to be "folded into" this new, smaller zone. This folding can cause certain superlattice states to occur at different points in k space than the corresponding bulk material states [28]. This can lead to direct transitions between materials which in the bulk form have indirect transitions. This has been demonstrated in the case of $GaAs_{0.4}P_{0.6}$/GaP and $GaAs_{0.2}P_{0.8}$/GaP superlattices, where both constituents are indirect in the bulk form [29]. Whether this is possible in the case of AlN/SiC is unknown, but very intriguing. It may be possible to obtain direct transitions throughout nearly the entire bandgap range with use of superlattices of AlN and SiC. Use of solid solutions in superlattices introduces additional degrees of freedom. For example, the bandgap can be varied independently of the lattice constant with proper choice of layer thickness and composition if superlattices of solid solutions of AlN and SiC were formed.

Due to the potential applications of solid solutions and superlattice structures of these two materials, an MBE/ALE system was commissioned, designed, and constructed for growth of the individual compounds of SiC and AlN, as well as solid solutions and heterostructures of these two materials. Dithisimal studies concerned with the kinetics and mechanisms of mass transport of Si, C, Al and N at the SiC/AlN interface are also being conducted in tandem with the deposition investigations.

A very important additional goal of this research is to understand what controls the contact electrical characteristics of specific metals to n-type 6H-SiC and to use this information to form good ohmic and Schottky contacts. A list of five metals to be studied, which consists of Ti, Pt, Hf, Co, and Sr, was created at the beginning of this research project. The selection process began by taking the simplest case, an ideal contact which behaves according to Schottky-Mott theory. This theory proposes that when an intimate metal-semiconductor contact is made the Fermi levels align, creating an energy barrier equal to the difference between the workfunction of the metal and the electron affinity of the semiconductor. It is the height of this barrier which determines how the contact will behave; for ohmic contacts it is desirable to have either no barrier or a negative barrier to electron flow, while for a good Schottky contact a large barrier is desired.

Although metals were chosen optimistically, i.e. on the basis that they will form ideal contacts, some evidence exists that the contact properties will be more complicated. J. Pelletier *et al.* [30] have reported Fermi level pinning in 6H-SiC due to intrinsic surface states, suggesting little dependence of barrier height on the workfunction of the metal. In addition, L. J. Brillson [31, 32] predicts the pinning rate to be higher for more covalently bonded materials. Other complications may arise if the surface is not chemically pristine. A major part of this project will be devoted to determining whether the contacts behave at all ideally, and if not, whether the Fermi level is pinned by intrinsic or extrinsic effects.

Along with examining the barriers of the pure metal contacts, the chemistry upon annealing will be studied and correlated with the resulting electrical behavior. The electrical behavior will be quantified both macroscopically in terms of current-voltage characteristics and micro-scopically in terms of barrier height. Identification of the phases formed will present the opportunity to attribute the electrical characteristics to the new phase in contact with silicon carbide.

Within this reporting period, the cleaning and etching of the vicinal α(6H)-SiC(0001) surface has been emphasized in this reporting period because of its recently demonstrated importance in the MBE of SiC and AlN films on SiC wafers and layers. Controlled growth of monocrystalline films of α(6H)(0001)- and β(3C)(111)-SiC has been achieved on α(6H)-SiC (0001) using disilane (Si_2H_6) and ethylene (C_2H_4) by gas-source molecular beam epitaxy at 1050°C–1150°C. The initial stages of AlN film growth has also been investigated in terms of defects via TEM. The interfacial chemistry and microstructure, electrical properties and the Schottky barrier heights of It thin films on α(6H)-SiC(0001) surfaces were investigated after annealing to 700°C and a maximum time of 60 min. The reaction zone contained Ti_5Si_3 and TiC. The electrical properties changed little as a function of heat treatment.

The experimental procedures, results, discussion of these results, conclusions and plans for future efforts for each of the topics noted above are presented in the following sections. Each of these sections is self-contained with its own figures, tables and references.

References

1. G. R. Fisher and P. Barnes, Philos. Mag. B **61**, 217 (1990).
2. H. P. Philipp and E. A. Taft, in *Silicon Carbide, A High Temperature Semiconductor*, edited by J. R. O'Connor and J. Smiltens (Pergamon, New York, 1960), p. 371.
3. W. von Muench and I. Pfaffender, J. Appl. Phys. **48**, 4831 (1977).
4. E. A. Bergemeister, W. von Muench, and E. Pettenpaul, J. Appl. Phys. **50**, 5790 (1974).
5. R. I. Skace and G. A. Slack, in *Silicon Carbide, A High Temperature Semiconductor*, edited by J. R. O'Connor and J. Smiltens (Pergamon, New York, 1960), p. 24.
6. W. von Muench and E. Pettenpaul, J. Appl. Phys. **48**, 4823 (1977).

7. S. Nishino, Y. Hazuki, H. Matsunami, and T. Tanaka, J. Electrochem Soc. **127**, 2674 (1980).
8. P. Das and K. Ferry, Solid State Electronics **19**, 851 (1976).
9. K. Sasaki, E. Sakuma, S. Misawa, S. Yoshida, and S. Gonda, Appl. Phys. Lett. **45**, 72 (1984).
10. P. Liaw and R. F. Davis, J. Electrochem. Soc. **132**, 642 (1985).
11. K. Shibahara, S. Nishino, and H. Matsunami, J. Cryst. Growth **78**, 538 (1986).
12. J. A. Powell, L. G. Matus, M. A. Kuczmarski, C. M. Chorey, T. T. Cheng, and P. Pirouz, Appl. Phys. Lett. **51**, 823 (1987).
13. H. S. Kong, Y. C. Wang, J. T. Glass, and R. F. Davis, J. Mater. Res **3**, 521 (1988).
14. J. A. Lely, Ber. Deut. Keram. Ges. **32**, 229 (1955).
15. H. S. Kong, J. T. Glass, and R. F. Davis, Appl. Phys. Lett. **49**, 1074 (1986).
16. H. S. Kong, B. L. Jiang, J. T. Glass, G. A. Rozgonyi, and K. L. More, J. Appl. Phys. **63**, 2645 (1988).
17. H. S. Kong, J. T. Glass, and R. F. Davis, J. Appl. Phys. **64**, 2672 (1988).
18. S. Kaneda, Y. Sakamoto, T. Mihara, and T. Tanaka, J. Cryst. Growth **81**, 536 (1987).
19. S. P. Withrow, K. L. More, R. A. Zuhr, and T. E. Haynes, Vacuum **39**, 1065 (1990).
20. C. F. Cline and J. S. Kahn, J. Electrochem. Soc, **110**, 773 (1963).
21. G. A. Slack, J. Phys. Chem. Solids **34**, 321 (1973).
22. W. M. Yim, E. J. Stofko, P. J. Zanzucci, J. I. Pankove, M. Ettenberg, and S. L. Gilbert, J. Appl. Phys. **44**, 292 (1973).
23. See, for example, R. Ruh and A. Zangvil, J. Am. Ceram. Soc. **65**, 260 (1982).
24. W. R. L. Lambrecht and B. Segall, Phys. Rev. B **43**, 7070 (1991).
25. T. L. Chu, D. W. Ing, and A. J. Norieka, Solid-State Electron. **10**, 1023 (1967).
26. R. F. Rutz and J. J. Cuomo, in *Silicon Carbide-1973*, ed. by R. C. Marshall, J. W. Faust, Jr., and C. E. Ryan, Univ. of South Carolina Press, Columbia, p. 72 (1974).
27. M. E. Sherwin and T. J. Drummond, J. Appl. Phys. **69**, 8423 (1991).
28. G. C. Osbourn, J. Vac. Sci. Technol. B **1**, 379 (1983).
29. P. L. Gourley, R. M. Biefeld, G. C. Osbourn, and I. J. Fritz, *Proceedings of 1982 Int'l Symposium on GaAs and Related Compounds* (Institute of Physics, Berkshire, 1983), p. 248.
30. J. Pelletier, D. Gervais, and C. Pomot, J. Appl. **55**, 994 (1984).
31. L. J. Brillson, Phys. Rev. B **18**, 2431 (1978).
32. L. J. Brillson, Surf. Sci. Rep. **2**, 123 (1982).

II. Surface Preparation of SiC Films

A. Introduction

SiC has properties which make it an attractive material for electronic devices used in high temperature and power applications. In order to make useful devices we need to be able to characterize the surfaces and be able to control surface properties. One parameter we wish to measure is the Schottky barrier height which results from a thin metal layer on a semiconductor. In the Schottky-Mott model, the barrier depends only on the work function of the metal and the electron affinity of the semiconductor. However, for most practical situations there will be a dependence on electronic states at the interface. These surface states result in a dipole at the interface and will substantially affect the Schottky barrier.

The Schottky barrier height (SBH) in diamond has been shown to depend significantly on surface preparation [1]. The same trend can be expected to hold for SiC. Thus, we focus on surface preparation of SiC as a means to control the SBH. Independent of model, the SBH for an n-type semiconductor is the difference between the metal Fermi level and the conduction band minimum, while for a p-type semiconductor the SBH is the difference between the Fermi level of the metal and the valance band edge.

The SBH can be deduced from Ultraviolet Photoemission Spectroscopy (UPS) measurements. The measurements involve directing 21.2 eV light (the He I resonance line) to the surface of the sample and counting the photo excited electrons as a function of electron kinetic energy. The measurement gives a profile of the valance band (VB) since the light promotes electrons from the VB to the conduction band (CB) by shifting the energy by 21.2 eV. From the spectra the VB edge can be determined from the onset of electron emis-sion. A thin metal layer can be then deposited on the semiconductor, and we can determine the Fermi level. Thus, the SBH for a p-type semiconductor can be measured directly. For an n-type semiconductor, the SBH is given by the bandgap energy minus the measured p-type barrier.

Before deposition of metals on the substrate, it is necessary to insure that a clean surface without defects or graphitization is obtained. We will examine cleaning both by *ex situ* wet chemical etch (HF spin) and *in situ* remote hydrogen plasma processing. Previous work dealing with *in situ* annealing indicated damage to the surface and an imbalance in the stoichometry. [2] The analytical tools used will be low energy electron diffraction (LEED), Auger electron spectroscopy (AES), Ultraviolet photoemission spectroscopy (UPS), and X-ray photoemission spectroscopy (XPS).

B. Experimental Procedure

The SiC samples used in this study were vicinal 6H n-type wafers supplied by Cree Research, Inc. The samples have doping concentrations of ~10^{15} to 10^{16} /cm^3. All work done

has been on the Si-terminated (0001) face which is oriented 3-4° towards [1120]. Prior to loading in the UHV system, the samples were prepared with an *ex situ* cleaning technique. The process included an HF spin etch with a solution of HF:H_2O:ethanol at 1:1:10. This technique was developed for the cleaning of Si wafers.

The surface analysis and *in situ* cleaning processes were carried out in an integrated surface processing/characterization system. The backbone of the system is a ~35ft. long UHV sample transfer system with eight stations. The eight stations include remote plasma cleaning, uv-photoemission, XPS, AES, LEED, Raman spectroscopy, temperature programmed desorption, and epitaxial metal deposition MBE.

After the *ex situ* surface preparation, additional surface cleaning was performed in the remote plasma chamber. The processing parameters were a pressure of 18 mTorr and a power output of 20 Watts; a flow of 10 sccm of hydrogen gas was employed and a plasma was excited by a rf-coupled source. The sample was heated to 400 °C prior to the plasma clean and held at that temperature for a one minute plasma cleaning. An earlier sample had been processed for ninety minutes. These two samples define limits for our process.

UPS measurements have been done on SiC samples as loaded, and after anneals of 700 °C and 1000 °C. The UPS chamber has a base pressure of 10^{-10} Torr. Operating conditions involve pressures up to 1×10^{-8} Torr, but the higher pressure is due to the helium inflow and does not contaminate the sample. As mentioned earlier, the UPS system utilizes a helium resonance lamp (the He I line) to provide a source of 21.2 eV light. The light is directed to the surface and electrons in the valence band can be promoted to the conduction band. Electrons from the conduction band can migrate to the surface and escape. Emitted electrons then are energy analyzed by a 50 mm radius hemispherical photomultiplier. Some low energy electrons are unable to overcome the electron analyzer work function and, thus, are not detected. A bias is applied to the sample to enable the low energy electrons to be detected.

In addition, X-ray photoemission spectroscopy was performed before and after plasma cleaning. XPS is similar to UPS but uses higher energy photons (~1487 eV). Due to the higher energies involved, the electrons detected originate from the core levels instead of the valence band. In principal, XPS is somewhat more sensitive to chemical composition than AES, and it displays chemical shifts which can be related to bonding configurations.

C. Results

Auger Electron Spectroscopy (AES) and Low Energy Electron Diffraction (LEED) were obtained immediately after loading the wafers into UHV and after a one minute H-plasma exposure at 400 °C. The AES spectra are compared in Fig. 1. As shown in the figure, the plasma processing sharply reduces the carbon and roughly halves the oxygen present at the surface. LEED measurements obtained immediately after loading showed no detectable

diffraction spots. In contrast, after the H-plasma exposure, a 1×1 hexagonal pattern was observed at an electron energy of 80 eV. The observation of a 1×1 pattern at this low electron energy indicates that the surface order has been substantially improved with the low temperature H-plasma clean.

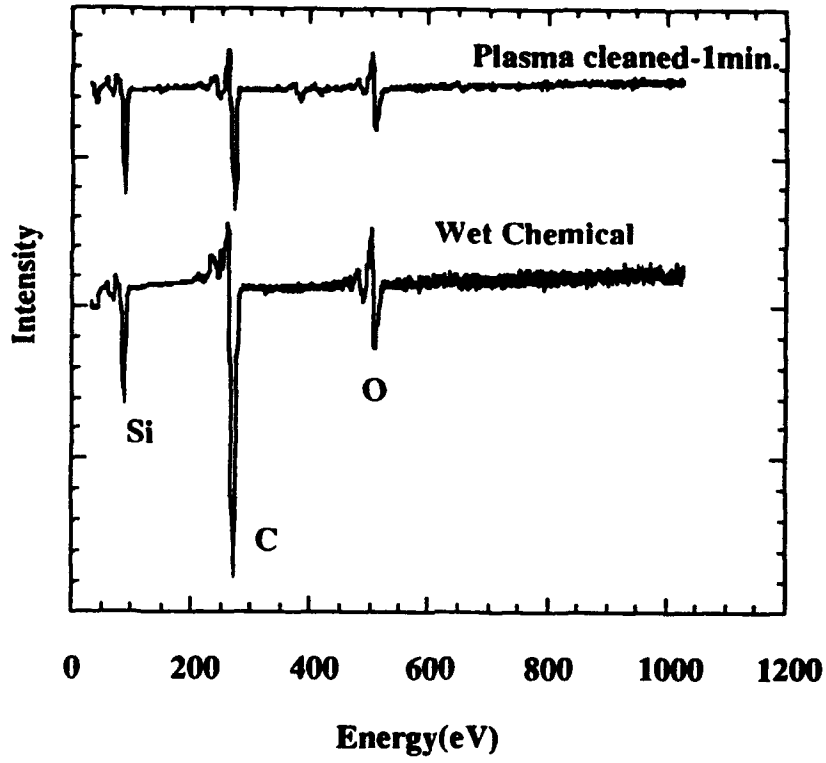

Figure 1. AES for SiC prepared with an *ex situ* chemical etch compared to a sample prepared with an *ex situ* etch plus an *in situ* H plasma clean. Spectra were normalized to the Si peak.

The XPS data also demonstrates the utility of the H-plasma cleaning. Figure 2 shows the Si 2s and 2p bands for the initial surface preparation and after H-plasma cleaning for a short and extended time. We note the Si lines are essentially unchanged in the process. The XPS spectra were also used to examine the C 1s transitions. The spectra are shown in Figure 3. The carbon 1s signal indicates two peaks present after the *ex situ* clean. After a short H-plasma exposure, the relative intensity of the higher energy feature is substantially reduced, and extended exposure results in complete removal of the feature. Recognizing that contamination due to hydrocarbon molecules at the surface is pervasive, we attribute this spectral change to hydrocarbon removal by the H-plasma.

The extended H-plasma exposure apparently also results in the removal of oxygen contamination. The results of the XPS measurements are summarized in Fig. 4. The spectra of the O 1s peak shows a doublet after the initial *ex situ* clean. After H-plasma exposure, one

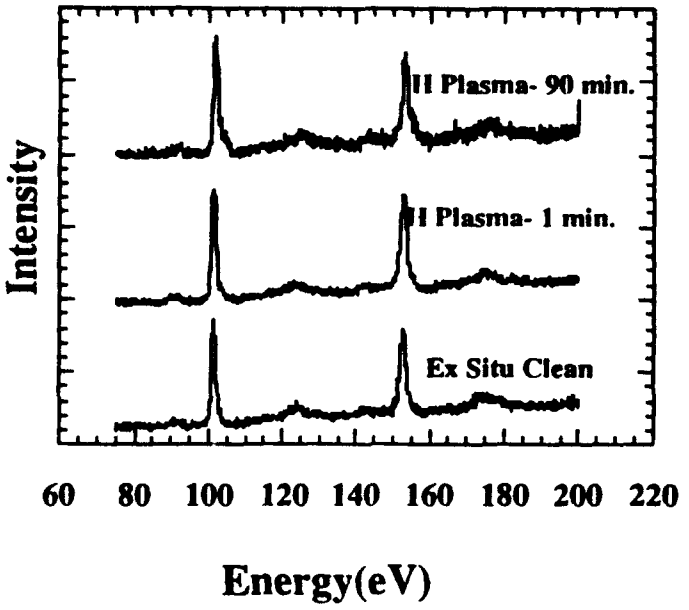

Figure 2. XPS data for the Si 2s and 2p peaks.

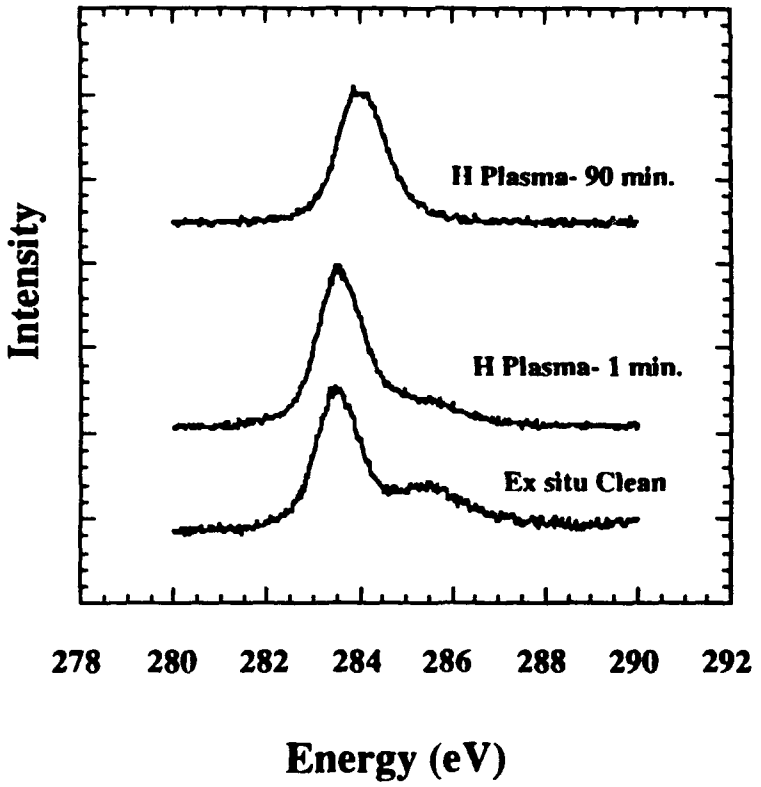

Figure 3. Carbon 1s peak.

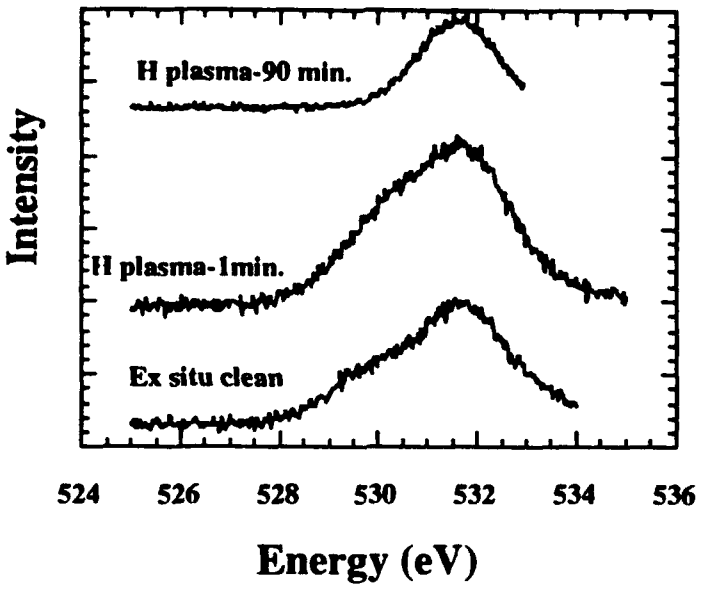

Figure 4. Oxygen 1s peak.

component of the doublet is substantially reduced. The origin of this doublet is not yet determined and will be the subject of future studies.

While annealing in UHV has previously been used to obtain clean surfaces, our previous UPS have shown that the processes tend to damage or disorder the surface. In contrast, the low temperature H-plasma cleaning procedure demonstrated here indicates that improved surface cleaning can be obtained with highly ordered surface structures.

D. Conclusions

Low temperature H-plasma processing for one minute has been shown to remove a significant amount of carbon and to remove 50% of the oxygen present on the SiC surface after HF etching. In light of these results, plasma cleaning appears as an attractive alternative to the standard annealing process of UHV annealing. It is projected that a five-minute plasma exposure will optimize the cleaning process. The 90-minute clean is considered too long to be practical. At present, we consider UHV annealing at elevated temperatures (~700 °C) to be undesirable, due to the formation of surface defects and damage.

E. Future Plans

The plasma chamber is being modified to use silane as a source gas. This will allow us to avoid preferential silicon evaporation at high temperature. The sample can then be heated, in a silane flow, to elevated temperature, giving off Si while Si is deposited and an equilibrium can be reached. With the results presented in this report, the interpolation is that a five-minute plasma exposure would optimize surface cleaning while keeping processing time short. UPS will be used to ensure that plasma processing has not damaged the surface. The *in situ* Raman

system mentioned in previous reports is operational and will be incorporated into the characterization of the SiC surface.

The Schottky barrier height (SBH) in diamond has been shown to depend significantly on surface preparation. The same trend can be expected to hold for SiC. Given this expectation, we will work further on surface preparation and cleaning. We will further investigate plasma cleaning of a bare SiC wafer and use the aforementioned silane treatment to try to arrive at a stoichometric surface with defect and impurity concentrations of less than 10^{12} cm^{-2}. Preliminary XPS data have been taken and we will incorporate XPS into future studies.

The last report focused on determining the electron affinity of AlN grown on SiC. This work continues in collaboration with Scott Kern.

F. References

1. J. van der Weide, R. J. Nemanich, Appl. Phys. Lett. **62**, 1878 (1993).
2. M. C. Benjamin, R. J. Nemanich ONR Semiannual Technical Report, June 1993.

III. Controlled Growth of the 3C and 6H Polytypes of SiC by Gas-source Molecular Beam Epitaxy

A. Introduction

Silicon carbide (SiC) is a wide band gap material that exhibits polytypism, a one-dimensional polymorphism arising from the various possible stacking sequences of, e. g., the silicon and carbon layers along the directions of closest packing. There are approximately 250 SiC polytypes [1]. Included in these is one cubic polytype. This single cubic polytype, β-SiC, crystallizes in the zincblende structure, has a room temperature band gap of 2.3 eV, and is commonly referred to as 3C-SiC. (In the Ramsdell notation, the three (3) refers to the number of Si and C bilayers necessary to produce a unit cell and the C indicates its cubic symmetry.) The other rhombohedral and hexagonal polytypes are classed under the heading of α-SiC. The most common of these latter polytypes is 6H-SiC with a room temperature band gap of ≈ 3.0 eV.

Since the 1950's, monocrystalline single crystals of 6H-SiC have been grown at using the Lely sublimation process [2]. However, nucleation was uncontrolled using this process and control of resultant polytypes was difficult. SiC single crystals inadvertently formed during the industrial Acheson process have also been used as substrates for SiC growth. However, neither these nor those formed using the Lely process are large enough for practical device applications. Recently, using a seeded sublimation-growth process, boules of single polytype 6H-SiC of >1 inch diameter of much higher quality of that obtained using the Lely process have been grown. The use of single crystals of the 6H polytype cut from these boules has given a significant boost to SiC device development.

SiC epitaxial thin film growth on hexagonal SiC substrates has been reported since the 1960's. The use of nominally on-axis SiC substrates has usually resulted in growth of 3C-SiC films. Films of 3C-SiC(111) grown by CVD have been formed on 6H-SiC substrates less than 1° off (0001) [3]. Films of 3C-SiC on 6H-SiC substrates have typically had much lower defect densities than those grown on Si substrates. The major defects present in β-SiC/6H-SiC films have been double positioning boundaries (DPB) [4]. Despite the presence of DPBs, the resultant material was of sufficient quality to further device development of SiC. The use of off-axis 6H-SiC(0001) substrates has resulted in growth of high-quality monocrystalline 6H-SiC layers with very low defect densities [5].

In addition, the use of more advanced deposition techniques, such as molecular beam epitaxy (MBE), has been reported for SiC in order to reduce the growth temperature and from about 1400–1500 °C on 6H-SiC substrates. Si and C electron-beam sources have been used to epitaxially deposit SiC on 6H-SiC (0001) at temperatures of 1150 °C [6]. Previous reports by all investigators have documented 3C-SiC growth only on 6H-SiC(0001) by MBE.

Ion-beam deposition of epitaxial 3C-SiC on 6H-SiC has also been obtained at the temperature of 750 °C using mass-separated ion beams of $^{30}Si^+$ and $^{13}C^+$.

Reflection high-energy electron diffraction (RHEED) at 10 kV and high-resolution transmission electron microscopy (HRTEM) were used for structure and microstructure analyses. Samples were prepared for HRTEM using standard techniques [7]. An Akashi EM 002B high-resolution transmission electron microscope was used at 200 kV for the HRTEM analysis.

B. Experimental Procedure

Thin, epitaxial films of SiC were grown on the Si and C faces of 6H-SiC(0001) substrates supplied by Cree Research, Inc. These vicinal 6H-SiC(0001) wafers oriented 3–4° towards [11$\bar{2}$0] contained a 0.8 μm epitaxial 6H-SiC layer deposited via CVD and a thermally oxidized 50 nm layer to aid in wafer cleaning. A novel *in situ* cleaning procedure has been developed using reaction and desorption of the silicon-containing precursor (Si_2H_6). This new procedure involves cleaning with 10% HF and a 10-minute anneal at 1050 °C in UHV, as well as a disilane exposure and boil-off. This additional cleaning step, intended to remove any residual oxygen, fluorine other contaminant and create a silicon terminated surface, exposes the substrate to 0.1 sccm Si_2H_6 for 2 minutes at 1050 °C until the surface undergoes a reconstruction from the 1×1 to 3×3 as observed by RHEED. This 3×3 reconstruction is indicative of a Si-rich surface. (For a description of the various surface reconstructions of SiC, please refer to Kaplan [9].) The 3×3 reconstructed samples were annealed at 1200 °C for 10 minutes causing them to revert to the 1×1 pattern.

All growth experiments were carried out in the gas-source molecular beam epitaxy system detailed in previous reports. The new heater assembly, designed for high temperature attainment and described in the previous report, has been installed and operates as expected allowing for substrate temperatures as high as 1400 °C. The sources of Si and C were Si_2H_6 and C_2H_4 (both 99.99% pure), respectively. Flow ratios of Si_2H_6 and C_2H_4 were varied from 1:2 to 1:1. Typical base pressures of 10^{-9} Torr were used.

C. Results and Discussion

All prior growth conditions have resulted, to this point, in monocrystalline, epitaxial layers of 3C-SiC with rough surfaces and the appearance of three-dimensional growth originating at the terraces of the vicinal substrates. The resulting films are generally cubic and have double positioning boundaries as evidenced by the RHEED and HRTEM. These results have been detailed in previous reports.

Single crystal layers of both 3C- and 6H-SiC have been grown on α(6H)-SiC(0001) by MBE (Fig. 1 shows a 6H- on 6H-SiC film. For a 3C- on 6H-SiC, please refer to previous

reports.) using a slightly modified procedure. Part of the new procedure involves the new cleaning procedure described in the previous section. Figures 2a and 2b show the 1×1 to 3×3 reconstructions, respectively.

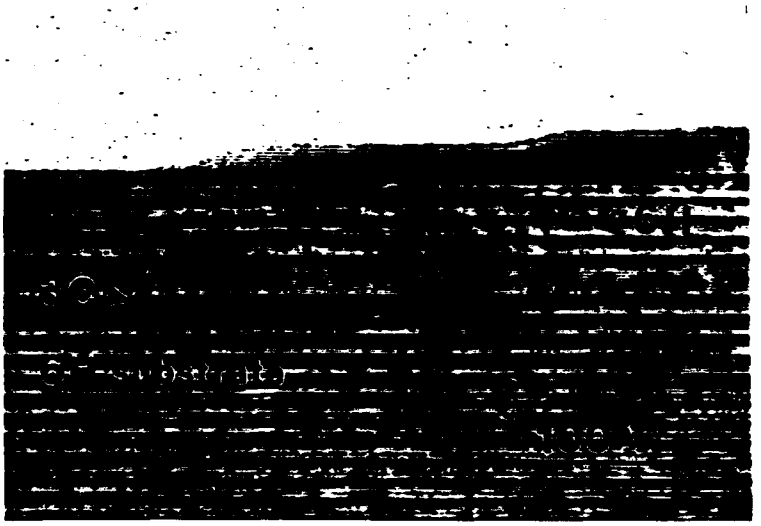

Figure 1. HRTEM micrograph showing a homoepitaxial film containing a mixture of 3C- and 6H-SiC on α(6H)-SiC(0001).

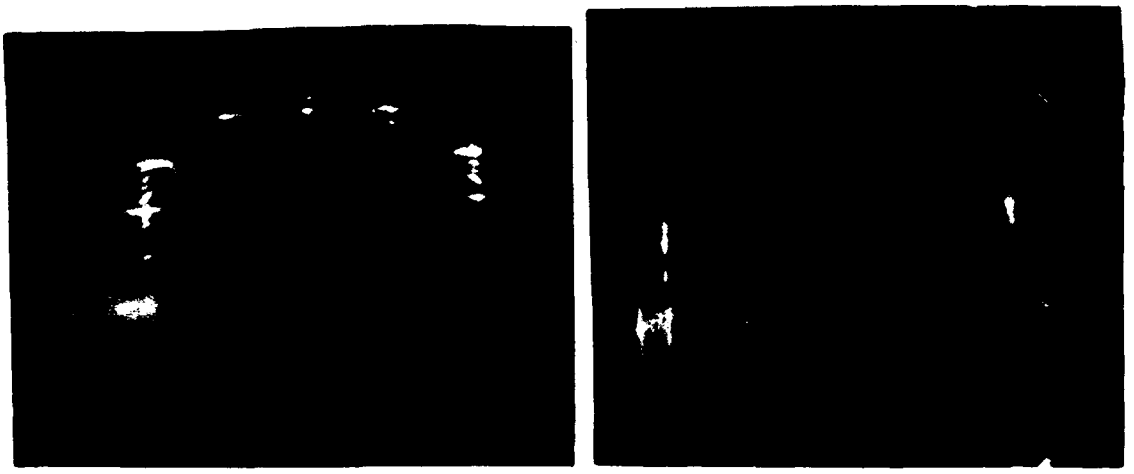

(a) (b)

Figure 2. RHEED photographs showing the reconstructions of the α(6H)-SiC(0001) surface (a) before exposure to disilane and after boil-off at 1200 °C and (b) after exposure.

Since all previous growth of SiC was done with 2-to-1 or higher C_2H_4-to-Si_2H_6 flow ratios and resulted in 3C-SiC films, the flow ratio was moved to 1-to-1 and the resulting films

are 6H. The film shown in Fig. 1 was grown at 1050 °C using the previously described pretreatment and flows of 0.1 sccm C_2H_4 and 0.1 sccm Si_2H_6 for 4 hours. This film has some regions of 3C-SiC, but the reason of formation is not yet known; however, other films grown under similar circumstances show no phase mixtures.

D. Conclusions

Preliminary studies into the surface science and growth conditions have been performed. The initial results indicate that the single most important factor in SiC polytype control (3C versus 6H) is the ratio of the precursor gases. Flow ratios of 1:1 lead to 6H-SiC films while carbon-rich ratios give 3C-SiC films. Another ongoing study involves the surface reconstruction phenomenon and its relation to film growth.

E. Future Research Plans/Goals

A new gas delivery system intended to allow for very low flow rates of an NH_3/Ar gas mixture is being installed so that an n-type dopant can be used easily. A study on both n- and p-type (with solid Al from a standard MBE effusion cell) is also underway. Further study of the effects of temperature, flow ratios and the role of surface reconstructions is also ongoing.

F. References

1. G. R. Fisher and P. Barnes, Philos. Mag. B **61**, 217 (1990).
2. J. A. Lely, Ber. Deut. Keram. Ges. **32**, 229 (1955).
3. H. S. Kong, J. T. Glass, and R. F. Davis, Appl. Phys. Lett. **49**, 1074 (1986).
4. H. S. Kong, B. L. Jiang, J. T. Glass, G. A. Rozgonyi, and K. L. More, J. Appl. Phys. **63**, 2645 (1988).
5. H. S. Kong, J. T. Glass, and R. F. Davis, J. Appl. Phys. **64**, 2672 (1988).
6. S. Kaneda, Y. Sakamoto, T. Mihara, and T. Tanaka, J. Cryst. Growth **81**, 536 (1987).
7. S. P. Withrow, K. L. More, R. A. Zuhr, and T. E. Haynes, Vacuum **39**, 1065 (1990).
8. J. C. Bravman and R. Sinclair, J. Electron Microsc. Tech. **1**, 53 (1987).
9. R. Kaplan, Surface Sci. **215**, 111 (1989).

IV. Initial Stage of AlN Film Growth on 6H-SiC by Plasma-Assisted Gas-source Molecular Beam Epitaxy

A. Introduction

It is of great importance to obtain atomically smooth surfaces and abrupt interfaces of heterostructural materials. The potential problems in the heteroepitaxial growth are mainly caused from lattice mismatches between the films and substrates [1]. This gives rise to some structural defect in the films such as misfit dislocations and misfit strains. In the case of AlN/SiC which has a 0.9% lattice mismatch, some defects have been reported to be caused by the surface structures of the substrates [2]. Moreover it should be significant to obtain not only defects free films but also atomically smooth films. For the growth of multilayered structures such as SiC/AlN/SiC, the smoothness of each layer would be especially desired. This feature in general is determined by growth modes, i.e. two-dimensional versus three-dimensional growth [3]. To obtain an atomically smooth surface, it should be necessary to grow films with a two-dimensional type of growth mode

In this study the initial stage of growth in terms of defects and surface morphology are investigated. HRTEM was utilized for this purpose.

B. Experimental Procedure

AlN films were grown on Si-faces of 6H-SiC (0001) substrates. The substrates used in this study were either on-axis or off-axis (3-4° off from (0001) toward $<11\bar{2}0>$) provided by Cree Research Inc. Films were all grown by a GSMBE method under the same conditions. The typical growth condition is shown in Table I. The details of the deposition can be seen in the accompanying report. In order to observe the initial stage of growth, the thickness of the films was controlled by varying the growth time.

Table I. Growth Conditions for the AlN films

Temperature	1050 °C
Al evaporation temperature	1260 °C
Nitrogen flow rate	3.5 sccm
Microwave power	100 W
Growth rate	17 Å/min

After growing the film, the sample was cut and glued face to face to make a cross-sectional TEM sample, followed by the thinning processes of grinding, dimpling and ion milling. Finally, the sample was examined by a Topcon EM-OO2B operated at a 200kV acceleration voltage.

C. Results

Figure 1 shows the cross-sectional image of a deposited AlN film on an on-axis 6H-SiC (0001) substrate. The surface is fairy smooth with only 10–20Å variation in thickness. Strains are periodically observed in the film corresponding mainly to the lattice mismatch between AlN and SiC of ~0.9%. Films grown on off-axis 6H-SiC showed similar features, implying a small affects of substrate orientation on surface morphology. It should, however, be noticed here that the defects observed in the film are strongly related to surface structures such as steps and terraces of the substrates.

Figure 1. Cross sectional TEM image of AlN film grown on 6H-SiC substrate.

Figures 2 (a) and (b) show the high resolution images of the interface regions of the on-axis and off-axis substrates, respectively. Epitaxial 2H AlN films which have an ABAB...stacking sequence can be clearly seen with the presence of some defects at the interface. There are considered to be two types of defects in the films. One is a misfit dislocation perpendicular to the substrate as indicated by arrow 1 in Fig. 2(a), which is produced by the lattice mismatch between AlN and SiC. The other is a planar defect parallel to the (0001) surface (arrow 2). The formation mechanisms will be discussed in the following section.

Figure 3 shows the initial stage of growth of the AlN film whose thickness is ~50Å. The film was grown on an off-axis 6H-SiC substrate. A rough surface texture can be seen, probably indicating island growth.

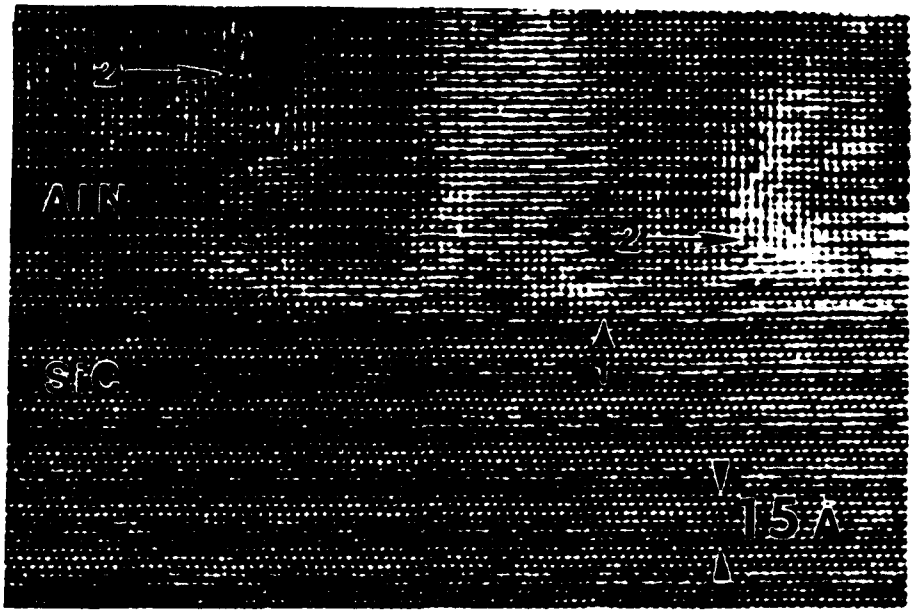

(a) on-axis substrate

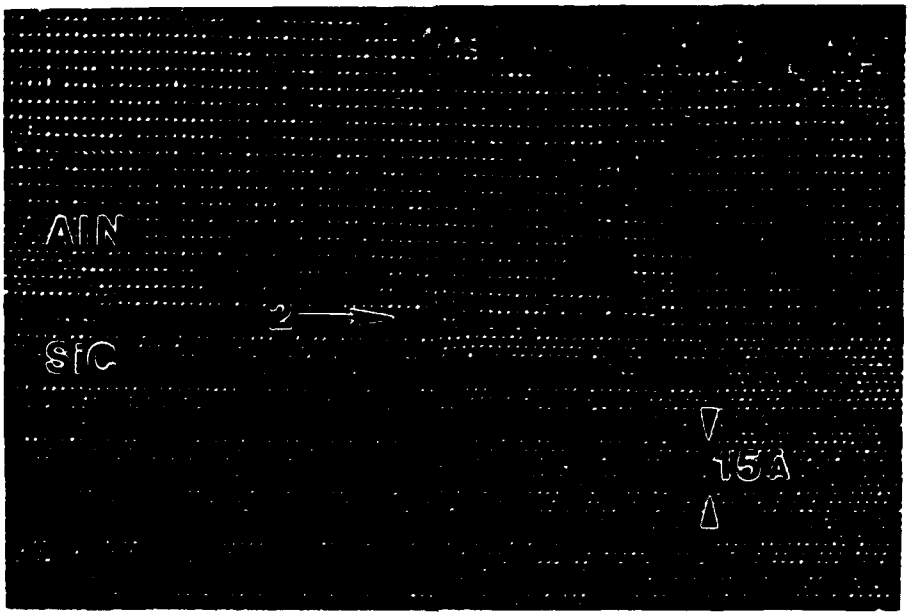

(b) off-axis substrate

Figure 2 HRTEM images of AlN/SiC interfaces of (a) on-axis and (b) off-axis SiC substrates. Arrow 1 and arrow 2 denote the misfit dislocation and the planar defects parallel to the surface, respectively.

D. Discussion

It is important to discuss the formation mechanisms of the defects observed in the film as described in the previous section. The initial stage of growth indicated that the film growth

Figure 3. HRTEM image of the initial stage of AlN growth. Island growth features can be observed.

probably commenced in an island growth mechanism. Surface energetic consideration can provide a certain idea of the growth mode thermodynamics [3]. However, one should be careful to apply this approach to this case because the growth is predominantly kinetically controlled.

The planar defects parallel to the surface are probably the results of coalescence between two nucleating islands. Nuclei on the different terrace sites, which are determined by the step heights of 6H-SiC substrate, fail to align with the neighboring nuclei (island) [4]. This misalignment causes the planar defects parallel to the surface. Thus, the existence of surface steps and the subsequent nucleation at these terrace sites can be potential at problem areas. This can explain the results of on-axis substrate because steps were also observed on the surface (Fig. 2(a)).

The formation of misfit dislocations can be understood in conjunction with the lattice mismatch between the film and the substrate. Since the critical thickness of the AlN/SiC system has not been obtained, a study should also be done on this topic. It may be useful to apply the strained super lattice idea [5].

E. Conclusion

The nature of the defects in AlN films grown by PAGSMBE was investigated through the observation of the initial stage of growth by cross-sectional HRTEM. Two types of defects were found. One was identified to be a misfit dislocations due to lattice mismatch between

AlN and SiC. The other originated from the coalescence of two islands which nucleated on the different terrace sites.

F. Future Research Plans

Attempts will be made to eliminate the density of the defect caused by the surface steps and island morphology. Misfit dislocations may be avoided below critical thickness. Since the critical thickness of AlN on SiC has not yet been obtained experimentally, this would be another goal of this study. Subsequently, a similar investigation should be made for SiC growth on AlN surfaces to complete pseudomorphic heterostructural studies.

G. References

1. Jan H. van der Merwe, Crit. Rev. Solid State Mater. Sci. 17(3), 187 (1991).
2. L. B. Rowland, R. S. Kern, S. Tanaka, and R. F. Davis, J. Mater. Res. 8(9), 2310 (1993).
3. E. Bauer and Jan H. van der Merwe, Phys. Rev. B 33, 3657 (1986).
4. H. L. Tsai and R. J. Matyi, Appl. Phys. Lett. 55, 265 (1989).
5. J. W. Matthews, A. E. Blakeslee, and S. Mader, Thin Solid Films 33, 253 (1976).

V. Chemistry, Microstructure, and Electrical Properties at Interfaces Between Thin films of Titanium and α(6H) Silicon Carbide (0001)*

L. M. Porter and R. F. Davis
Department of Materials Science and Engineering, North Carolina State University, Raleigh, NC 27695-7907

J. S. Bow, M. J. Kim, and R. W. Carpenter
Center for Solid State Science, Arizona State University, Tempe, AZ 85287-1704

R. C. Glass
Westinghouse Science and Technology Center, Westinghouse Corporation, Pittsburgh, PA

Abstract

Thin films (4 – 1000Å) of Ti contacts deposited via UHV electron beam evaporation at room temperature on monocrystalline, n-type, alpha (6H)-SiC (0001) were epitaxial. Current-voltage (I-V) measurements showed that the Ti contacts were rectifying with low ideality factors ($n < 1.09$) and typical leakage currents of 5×10^{-7} A/cm^2 at -10 V. The Schottky barrier heights (SBH's) calculated from x-ray photoelectron spectroscopy and I-V and C-V measurements were between 0.79 and 0.88 eV.

The interfacial chemistry and microstructure, electrical properties, and SBH's were investigated after annealing at 700°C up to 60 min. High resolution TEM analyses indicated that the reaction zones consisted of Ti_5Si_3 and TiC. The corresponding electrical properties exhibited considerable stability except after an initial 20 min. anneal.

*Paper submitted to Journal Materials Research

A. Introduction

The extreme thermal, mechanical, and electronic properties of SiC has allowed its use for both structural applications and high-power, -temperature, -speed, and -frequency electronic and optoelectronic devices. The chemistry at annealed Ti/SiC interfaces has been investigated for structural applications by many groups, as discussed below. However, no integrated study has been found which has examined the Ti/SiC interface in terms of the chemistry, microstructure, and electrical properties for the purpose of contacts in semiconductor devices.

The increased use of (6H)-SiC for many types of semiconductor devices is challenged by the difficulty of controlling the properties of the metal contact/SiC interface, including uniformity and thickness of the interfacial region, stability at high temperatures (~600°C), and most importantly, the Schottky barrier height (SBH), or the energy barrier for electrons traversing the interface. It is important to understand the chemistry and microstructure at the interface between the metal contact and the SiC substrate before and after annealing at temperatures at or above which devices may be operated so that the resulting phases may be correlated with the electrical properties.

In this study, analytical techniques have been employed to investigate the interfacial chemistry and microstructure on both an atomic scale and a microscopic (<1 μm) scale between Ti and n-type 6H-SiC (0001) before and after annealing at 700°C. In addition, the chemically-cleaned SiC surface was characterized in terms of chemistry, structure, and amount of band bending. The results of these studies have been correlated with the electrical properties and SBH's of the Ti contacts.

B. Experimental Procedure

SiC Material & Preparation. Vicinal, single crystal, nitrogen-doped, n-type ($\approx 10^{18}$ cm^{-3}) wafers of 1" diameter 6H-SiC (0001) containing 0.5-1.5 μm thick, n-type ($\approx 10^{16}$–10^{17} cm^{-3}) homoepitaxial films thermally oxidized to a thickness of 500-1000Å in dry oxygen at 1300°C were provided by Cree Research, Inc. The epitaxial layers were unintentionally-doped. The Si-terminated (0001) surface, tilted 3°–4° towards [1$\bar{2}$0] was used for all depositions and analyses.

The substrates were simultaneously cleaned and the oxide layer etched from the surface using a 10 min. dip in either an ethanol / hydrofluoric acid / water (10:1:1) or 10% hydrofluoric acid solution. This was followed by a quick rinse in deionized water. The substrates were loaded immediately into a vacuum system transfer tube (base pressure $\approx 10^{-9}$ Torr), thermally desorbed at 700°C for 15 min. to remove any residual hydrocarbon contamination, and transferred to the metal deposition chamber.

Metal Deposition. A UHV electron beam evaporation system was used to deposit various metal films having thicknesses ranging from 4–1000 Å onto the substrates described above.

A substrate manipulator allowed for both heating and rotation and contained a manual shutter directly below the position of an inverted Mo substrate block located in the upper part of the chamber. The contact metals were evaporated using a dual source 270°, 10 cc electron beam evaporator made by Thermionics Corporation. A 330 l/s turbomolecular pump was used for roughing the system and during processing. A 500 l/s diode ion pump and a titanium sublimation pump were employed to achieve and maintain UHV base pressures of $<2\times10^{-10}$ Torr.

Prior to deposition, approximately 25–50 Å was typically evaporated from the source to liberate any foreign material which may have collected on its surface. Each substrate was covered by the shutter during this operation. To commence the deposition, the emission current was increased very slowly until a deposition rate of 10–12 Å/min was stabilized according to the XTC thickness monitor, and the shutter subsequently removed from in front of the sample. The pressure during the depositions was between 5×10^{-9} and 5×10^{-8} Torr. The Ti acted as a pump during evaporations such that the pressure dropped slowly. After ≈ 100 Å was deposited, the rate was typically increased to ≈ 20 Å/min. Throughout each deposition the substrates were rotated to ensure uniform thickness across the sample. The substrates were not intentionally heated.

Analysis Techniques. Patterned contact structures consisting of 500 μm (0.02") and 750 μm (0.03") diameter circular contacts of 100 nm thickness were created by depositing the metal through a Mo mask in contact with the SiC epitaxial layer for electrical characterization. Silver paste served as the large area back contact. All subsequent annealing was conducted in UHV. Current-voltage (I-V) measurements were taken with a Rucker & Kolls Model 260 probe station in tandem with an HP 4145A Semiconductor Parameter Analyzer. Capacitance-voltage (C-V) measurements were taken with a Keithley 590 CV Analyzer using a measurement frequency of 1 MHz.

Titanium/SiC samples were prepared in cross-section for analysis by transmission electron microscopy (TEM). High resolution (HR) images were obtained with an ISI EM 002B operating at 200 kV with an interpretable resolution limit of 0.18 nm. These images were typically recorded at an electron-optical magnification of 490,000 to 590,000. Some of the HRTEM micrographs were digitized using a 512×512 camera and the resulting images analyzed by using the SEMPER program [1]. Lattice spacings (d-spacings) and interplanar angles were measured from optical digital diffraction patterns and used to identify the reaction product phases. The values of the lattice spacings were calculated using the (0006) d-spacing in 6H-SiC measured near the phase to be identified as a baseline. Thus, the change in d-spacing due to different fucusing conditions was negligible. A data base of d-spacings for each possible reaction product phase was compared to the experimentally-determined d-spacings. The d-spacings from the data base which were within 2% of the measured values were compared with interplanar angles for the identification of phases. Most of the measured

values were within 1% of the theoretical values. Unknown phases were identified uniquely by these procedures.

Analytical electron microscopy was performed using a Gatan 666 parallel electron energy loss spectrometer (PEELS) with spatial resolution of approximately 3 nm attached to a Philips 400 FEG operating at 100 kV. Energy dispersive spectrometry (EDS) was performed using a JEOL 2000 FX operating at 200 kV with a probe size of approximately 40 nm. For fixed position PEELS and EDS, the probe position was adjusted in the diffraction mode by monitoring the shadow image in the Bragg disk of the transmitted beam. The image was created by defocusing the second condenser lens. A liquid nitrogen cooled double-tilted holder was used for all analytical experiments to minimize specimen contamination and local specimen heating.

Surface chemistry was studied using a Riber x-ray photoelectron spectroscopy (XPS) system. This system consists of a Mac2 semi-dispersive electron energy analyzer and is accessible by UHV transfer from the deposition chamber. Using Mg Kα (1253.6 eV) x-rays, the x-ray source was operated at 14 kV with an emission-controlled current of 15 mA. This technique also allowed the calculation of the Schottky barrier height for thin films of Ti on SiC.

Analyzing samples usually consisted of three different types of spectra. Survey scans, which were important for fingerprinting elements present at the surface, contained 2000 data points from 0 to 1000 eV and were obtained 2.0 eV resolution and a counting rate of 100 ms. Scans of individual photoelectron peaks at higher resolution (0.8 eV) contained 500–750 data points and a 20-30 eV binding energy range. Valence spectra contained 500 data points from 0 to 20 eV and contained 500 data points at a resolution of 0.8 eV.

C. Results and Discussion

Surface Chemistry. Comparison of the XPS C 1s and Si 2p peak areas divided by their atomic sensitivity factors revealed that chemically-cleaned, *non*-thermally oxidized SiC substrates contained C-rich surfaces. Thermal oxidation and subsequent etching solved this problem. This indicates that the excess C was present only at the surface and occurred during the cessation of the growth process. As such, all as-received SiC substrates used in this research contained a thermally-grown oxide.

X-ray photoelectron spectroscopy was also used to monitor the surface chemistry after cleaning. Figure 1 shows survey spectra after three different cleaning procedures. All cleaning procedures consisted of etching the oxide in a hydrofluoric acid solution followed by either a chemical or thermal process to remove hydrocarbon contamination. The top spectrum represents a sample which was etched for 10 min. in a 10% HF aqueous solution, quickly rinsed in deionized water, and heated to 700°C for 15 min.

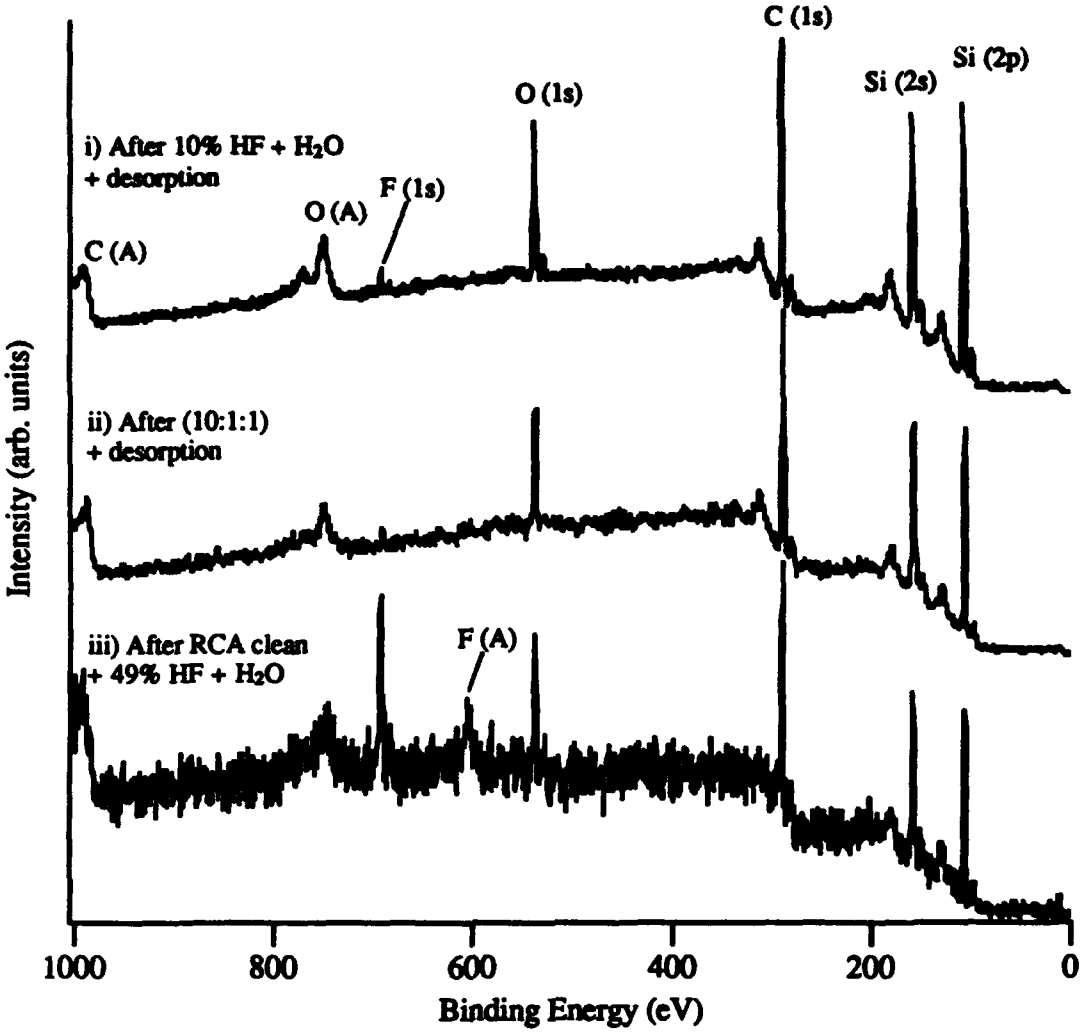

Figure 1. XPS survey spectra of the (0001) SiC surface after i) 10 min. in 10% HF and a quick deionized water rinse followed by a 15 min. UHV desorption at 700°C, ii) 10 min. in a (10:1:1) solution of ethanol / HF / deionized water followed by a 15 min. UHV desorption at 700°C, and iii) a modified RCA clean followed by 10 min. in 49% HF and 5 min. rinse in deionized water.

The spectrum shows that residual oxygen and, to a lesser extent, fluorine remained on the surface. The peaks marked with '(A)' are Auger peaks. A comparison of the relative concentrations of the elemental constituents requires incorporating both the peak area and the peak area sensitivity, or atomic sensitivity factor. The relative concentrations of the elements comprising the photoelectron signal can be estimated from the following expression [2]:

$$C_x = \frac{I_x / S_x}{\sum_i I_i / S_i}, \qquad (1)$$

where I is the integrated peak area and S is the atomic sensitivity factor. However, this

expression does not take into account the fact that top portion of a film contributes to more of the signal than the portion underneath. The concentrations are relative to the total signal and not to an actual volume at the surface. The atomic sensitivity factors are 0.205 for C 1s, 0.63 for O 1s, 1.00 for F 1s, and 0.17 for Si 2p [2]. Using Eq. 1, the relative concentrations calculated from these sensitivity factors with their respective peak areas were (± 1%) 49.7% Si, 40.0% C, 9.3% O, and 0.9% F. It is believed that the higher concentration of Si as compared to C is representative of a Si-terminated surface. Waldrop et al. [3] calculated the amount of O on the same type of substrates to be ≈ 3/4 monolayer in addition to a trace amount of F (F/O < 0.05).

The middle spectrum represents a sample which was prepared by the same procedure noted above except a (10:1:1) ethanol / hydrofluoric acid / deionized water solution was used in place of the 10% HF solution. Descriptions of using this solution for cleaning Si can be found in Ref. 4. The survey spectrum does not show any significant change in the amounts of O and F. The relative concentrations in this case were 45.8% Si, 44.8% C, 8.9% O, and 0.5% F. The C concentration is higher than in the case above because the sample was not thermally oxidized before surface treatment.

Results from a third cleaning procedure are shown in the bottom spectrum. This sample was first RCA cleaned, the sequence of which consisted of a 5 min. dip in a (1:1:5) solution of NH_4OH / H_2O_2 / H_2O (70°C), a 5 min. rinse in deionized water, a 5 min. dip in a (1:1:5) solution of HCl / H_2O_2 / H_2O (70°C), and a 5 min. rinse in deionized water. The sample was then etched in a 49% HF aqueous solution for 10 min. and rinsed in deionized water for 5 min. The survey shows that the higher concentrated HF solution resulted in a substantial increase in the amount of F left on the surface. The relative concentrations were 41.2% Si, 42.9% C, 8.5% O, and 7.3% F. It should also be mentioned that although this cleaning procedure did not consist of a thermal desorption, no significant changes in the amounts of O and F were found before and after the thermal desorptions for the preceding two procedures. Because of these results, the solutions containing lower HF concentrations were used for samples prior to metal deposition.

Figure 2 shows XPS Si 2p and C 1s spectra of a SiC surface that has been treated in 10% HF. Spectra of the surface before and after desorption at 700°C are compared. The Si 2p peaks before and after desorption appear to be virtually identical. Deconvolution of these peaks revealed both the main Si (bound to C) peak at 101.58 eV and a small peak at 102.98 eV, which is attributed to SiO_x [5]. The C peak does show significant change after desorption. The main peak at 283.78 eV is due to C bound to Si in SiC [6]. Before desorption a significant peak exists on the high binding energy side of the main peak and is attributed to adventitious carbon, which has a binding energy of 285.0 eV [7].

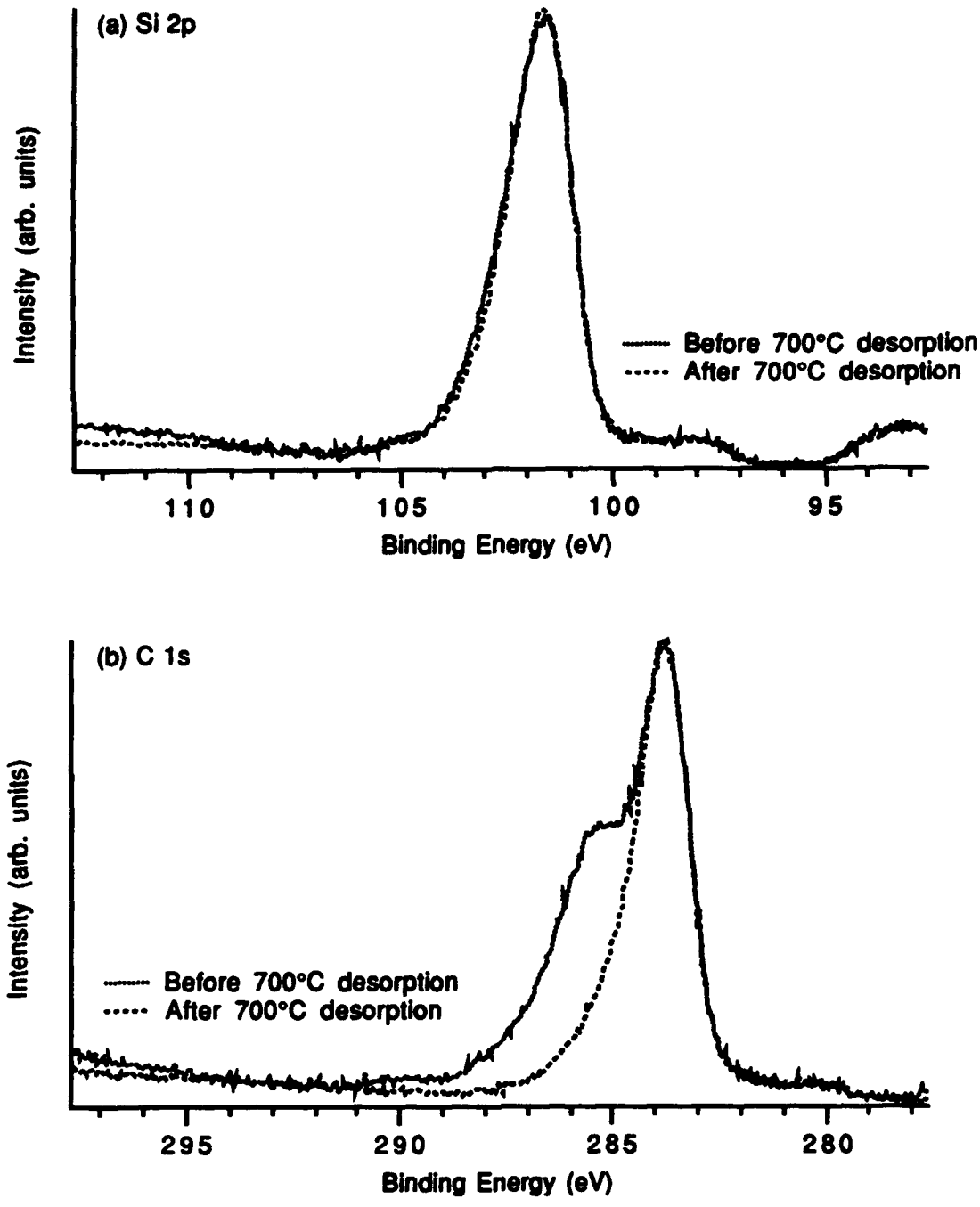

Figure 2. XPS spectra of 6H-SiC (0001) after 10 min. in 10% HF followed by a deionized water rinse. The (a) Si 2p and (b) C 1s peaks before and after a 700°C desorption are shown.

Surface Structure. The surface structure was monitored by low energy electron diffraction (LEED). For all samples examined treated by the various cleaning procedures noted above, a 1×1 unreconstructed surface was displayed. This result is in agreement with that of Waldrop *et al.* [3] where 3/4 monolayer O and trace F was left on the Si-terminated surface of 6H-SiC.

As suggested by Kaplan [8], a 1×1 surface probably corresponds to a range of structures which do not have long range order. The 1×1 patterns in this case are most likely due to adsorbed O and F.

Titanium/Silicon Carbide Interfaces. Electrical Properties. Current-voltage measurements of Ti contacts deposited at room temperature on n-type SiC (0001) were rectifying with low ideality factors (n<1.09) and with typical leakage currents of 5×10^{-7} A/cm^2 at -10 V. Figure 3 shows a representative I-V characteristic of an as-deposited, 2.0×10^{-3} cm^2 Ti contact. The reverse bias characteristics of the same contact did not show hard breakdown to 100V, which is the voltage limit of the equipment. Instead, the leakage steadily increased to ≈ 35 μA. This 'soft breakdown' is expected from high fields at the contact edges due to the geometry of the contact structure. It is not believed that inhomogeneities in the interface structure are the cause of the increasing leakage [9] because of the nature of this interface, which is described in the following section.

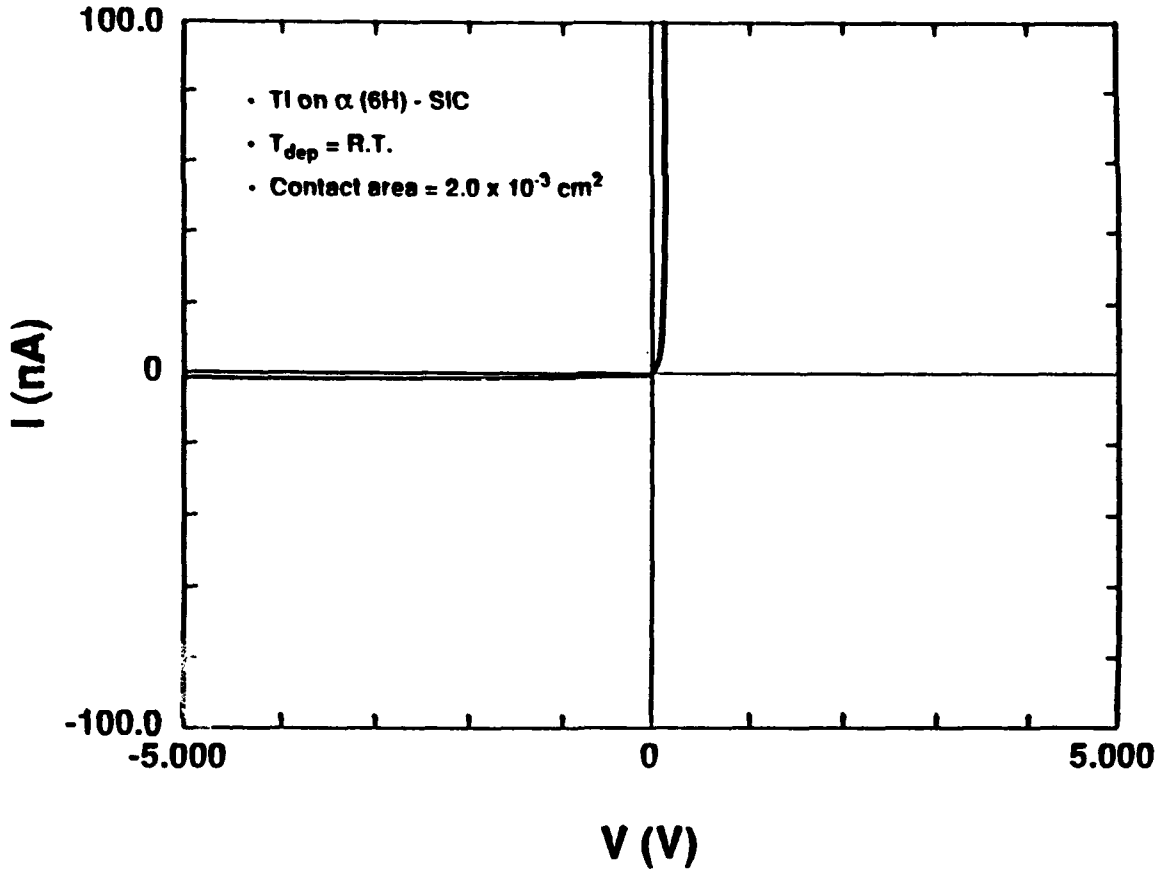

Figure 3. Current-voltage characteristics of Ti deposited on 6H-SiC at toom temperature. (contact area = 2.0×10^{-3} cm^2).

For values of applied voltage, V, greater than 3kT/q, the current density can be expressed as

$$J = J_s \exp\left(\frac{qV}{nkT}\right), \tag{2}$$

where J_s, is the extrapolated current density at zero voltage or saturation current density, and n is the ideality factor. Therefore, the ideality factor can be calculated from the linear region of a semi-logarithmic plot of current vs. voltage, as displayed in Fig. 4. The linear region in this case extends over approximately four decades of current. The reduced slope at higher voltages is due to the resistance of the substrate material. The low ideality factors were taken as evidence that thermionic emission theory may be applied for calculating the SBH.

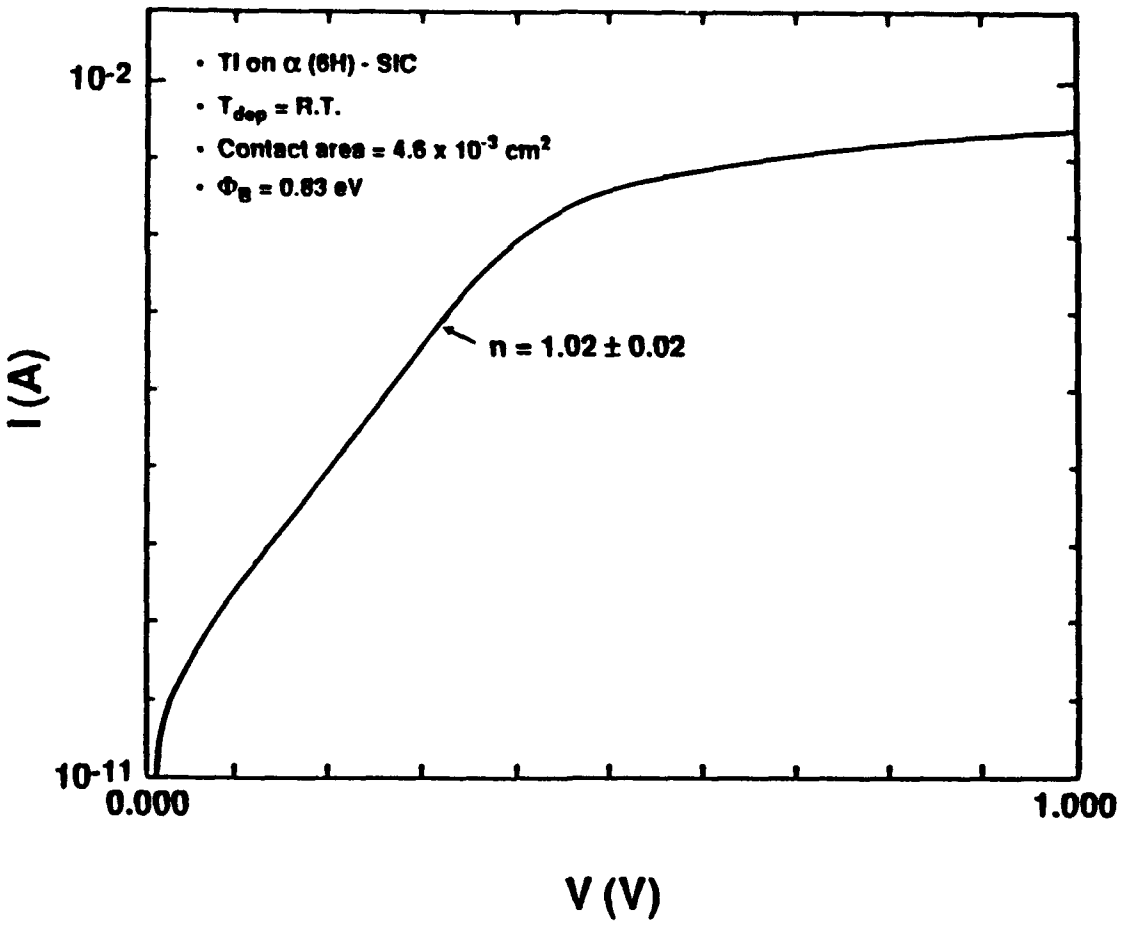

Figure 4. Semi-logarithmic I-V plot of Ti deposited on 6H-SiC. (contact area = 4.6×10^{-3} cm^2)

Following Eq. 2 the SBH can then be determined from the equation

$$\Phi_B = \frac{kT}{q}\ln\left(\frac{A^*T^2}{J_s}\right), \tag{3}$$

where A* is the effective Richardson constant. The value of A* for 6H-SiC is 194.4 A/cm^2/K^2 [10]. The accuracy of A* is not usually critical, since, at room temperature, doubling its value only increases Φ_B by 0.018 eV [11]. Using this equation with $J_s = 2.0\times10^{-7}$ A/cm^2, a SBH of 0.83 eV was calculated for unannealed Ti contacts.

The barrier heights were also determined from C-V measurements. Plotting $1/C^2$ vs. V allows the barrier height to be determined from the equation

$$\Phi_B = V_i + \xi + \frac{kT}{q} - \Delta\Phi, \tag{4}$$

where V_i is the voltage intercept; ξ, is the difference between the conduction band and the Fermi level in the bulk of the material and is a function of the carrier concentration; and $\Delta\Phi$ is the image force lowering. Figure 5 shows $1/C^2$ vs. V of an as-deposited Ti/SiC contact biased from 0 to -5 V. Extrapolating the linear region gives an intercept of 0.67 V, indicating a SBH of 0.88 V.

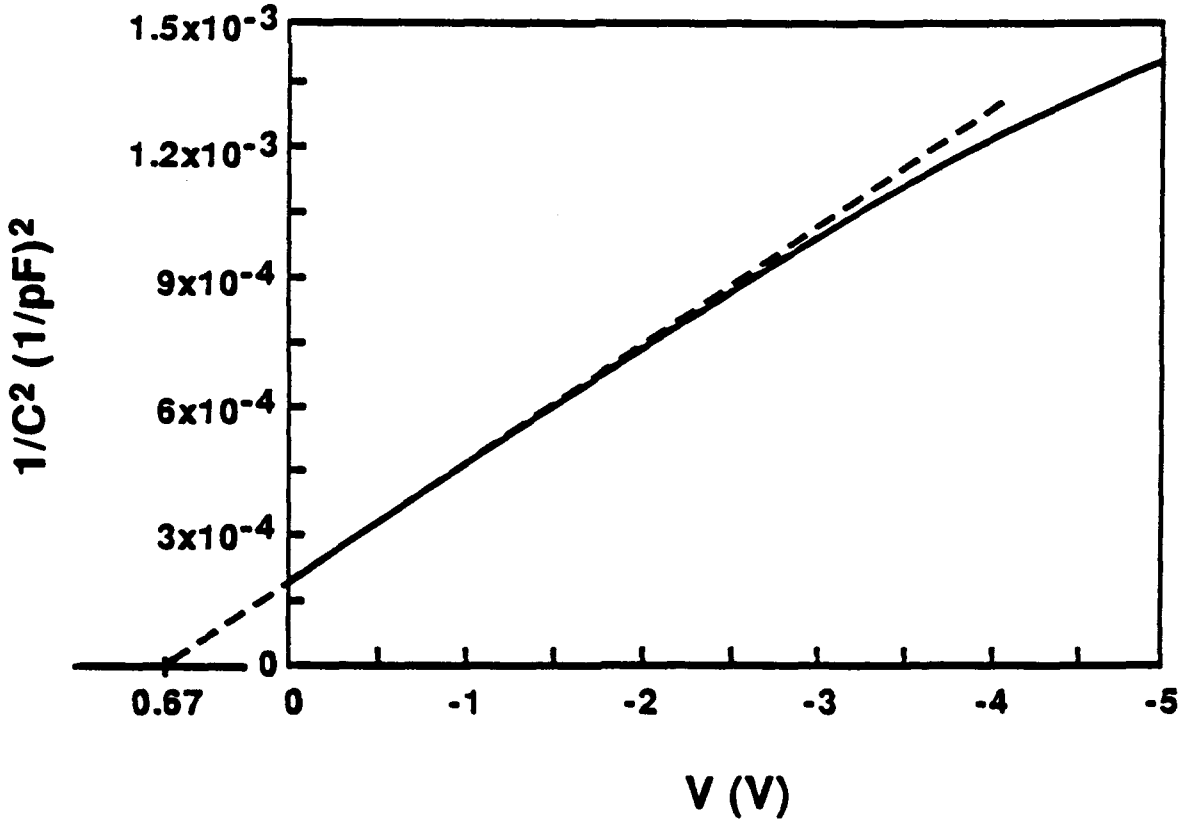

Figure 5. $1/C^2$ vs. V plot of as-deposited Ti/SiC. (contact area = 2.0×10^{-3} cm^2)

After annealing at 700°C for 20 minutes, the leakage increased; however, after further annealing to 60 minutes the characteristics in terms of leakage and ideality factors again improved. The I-V characteristics through the annealing series are plotted in Fig. 6. It can be seen from the corresponding semi-logarithmic plot (Fig. 7) that there was no linear region after annealing for 20 min. However, the ideality factors returned to low values ($n<1.09$) after further annealing. The barrier heights after annealing for 40 and 60 min. were 0.86 and 0.90 eV, respectively. The SBH after annealing for 60 min. was calculated from C-V measurements to be 1.04 eV.

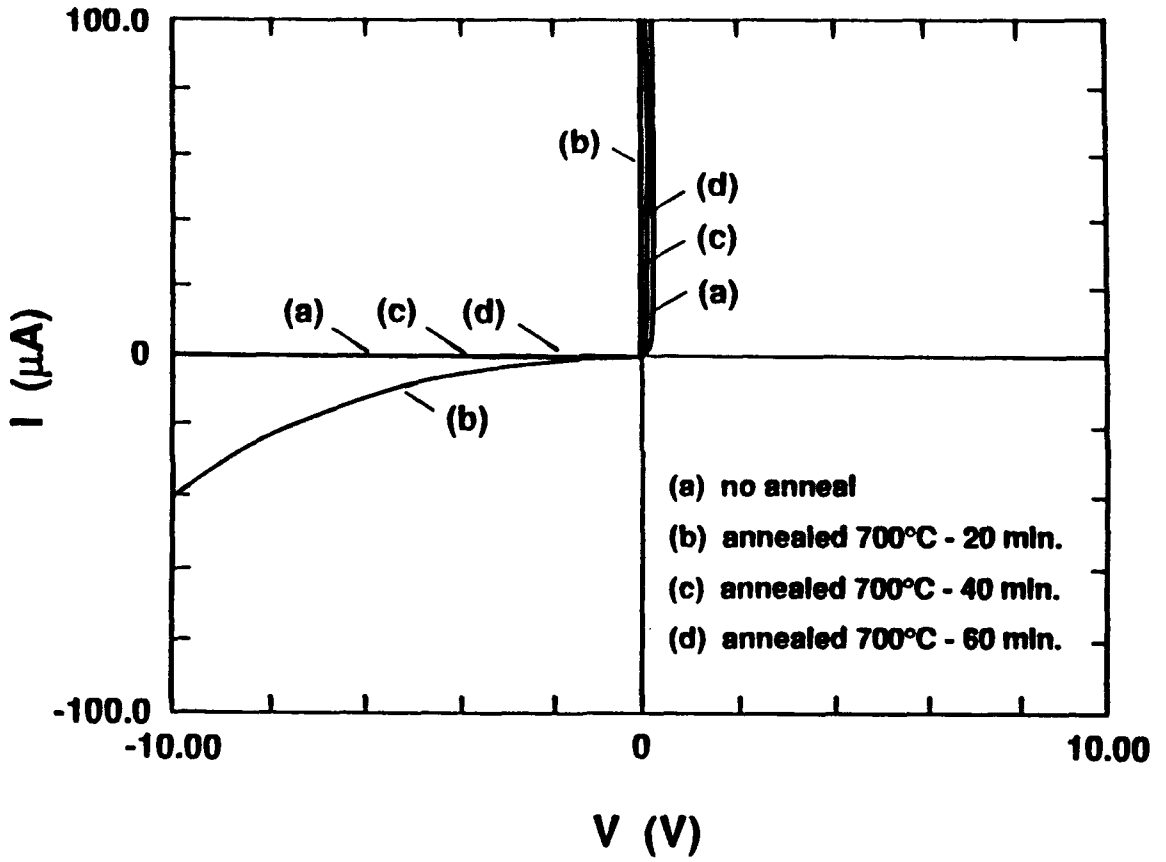

Figure 6. Current-voltage characteristics of Ti/SiC after annealing at 700°C. (contact area = 2.0×10^{-3} cm^2)

The Schottky barrier height was also calculated from XPS spectra by careful comparison of core level peaks before and after deposition of very thin Ti films. In these experiments core level and valence band spectra were obtained of the SiC surface after chemical and thermal cleaning and prior to metal deposition. Immediately following the SiC surface analysis, a sequence of metal depositions was performed, which resulted in films of total thicknesses between 4 and 12 Å.

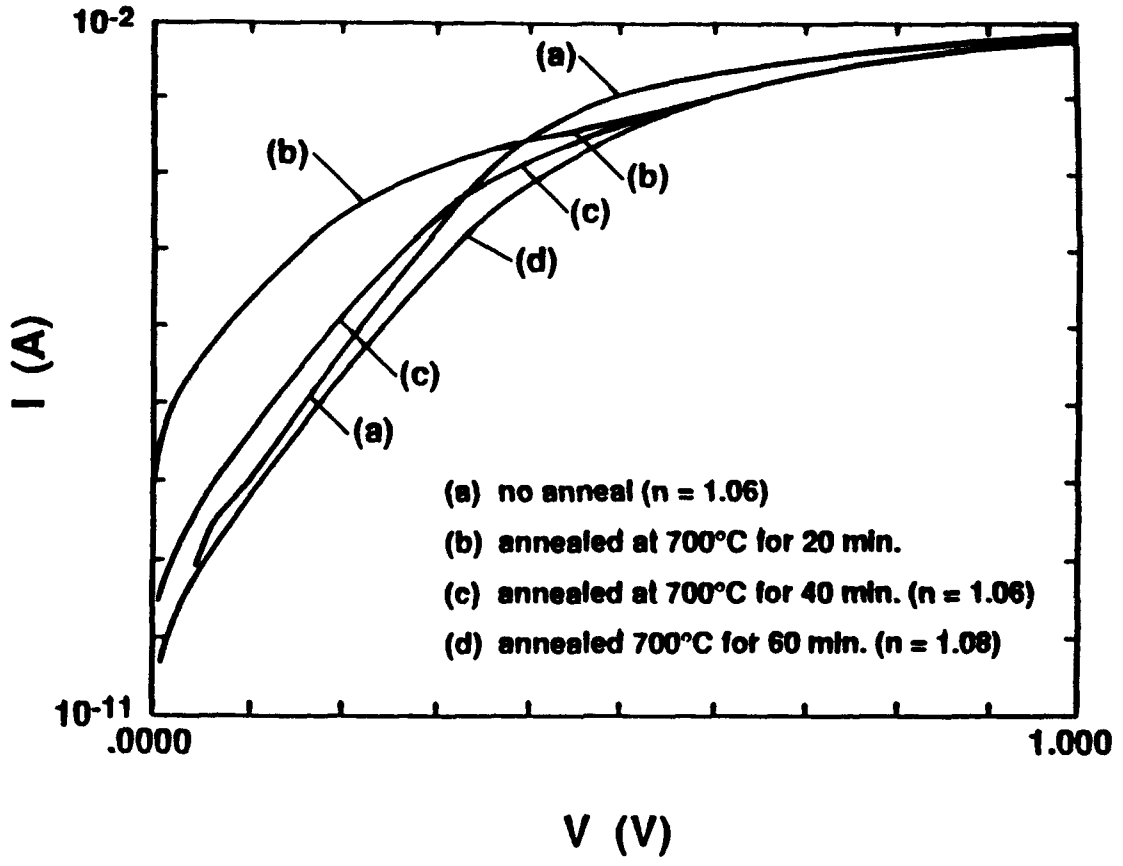

Figure 7. Semi-logarithmic I-V plot of Ti/siC after annealing at 700°C. (contact are = 2.0×10^{-3} cm^2)

The binding energy (BE) of a photoelectron is related to its kinetic energy (KE) by the following relationship:

$$E_B = h\upsilon - E_K - \Phi_S, \tag{5}$$

where hν is the energy of the x-ray photons, E_K is the kinetic energy of the emitted electrons, and Φ_S is the work function of the spectrometer (analyzer). The value of binding energy which is obtained directly from an XPS scan is actually equal to the true binding energy, BE, plus Φ_S. Because binding energies are defined with respect to the Fermi level, it is important to use a known standard to define the Fermi level position. If the work function of the spectrometer tends to drift, a standard should be used with each collection of data. In these experiments a piece of Au foil was used as a standard with each new series of data. The Au $4f_{7/2}$ peak has a known binding energy of 84.00 eV. The measured value of the Au $4f_{7/2}$ peak is equal to 84.00 eV plus the work function of the spectrometer. Therefore, the measured binding energies of all core levels are corrected by the work function of the spectrometer determined from the Au standard. In this system the spectrometer work function was usually 4.0 ± 0.2 eV (Au $4f_{7/2}$ at ≈ 88.0 eV).

The relationship between the SBH and the values measured by XPS is shown in Figure 8. This diagram shows energy bands in 6H-SiC which bend upward at the surface due either to surface states or to the metal contact. In nominally-doped material, which was used in these experiments, the depth over which band bending (>1000 Å) occurs is much larger than the photoelectron escape depth (≈ 20 Å); therefore, the XPS spectra effectively represent the position of energy bands at the surface.

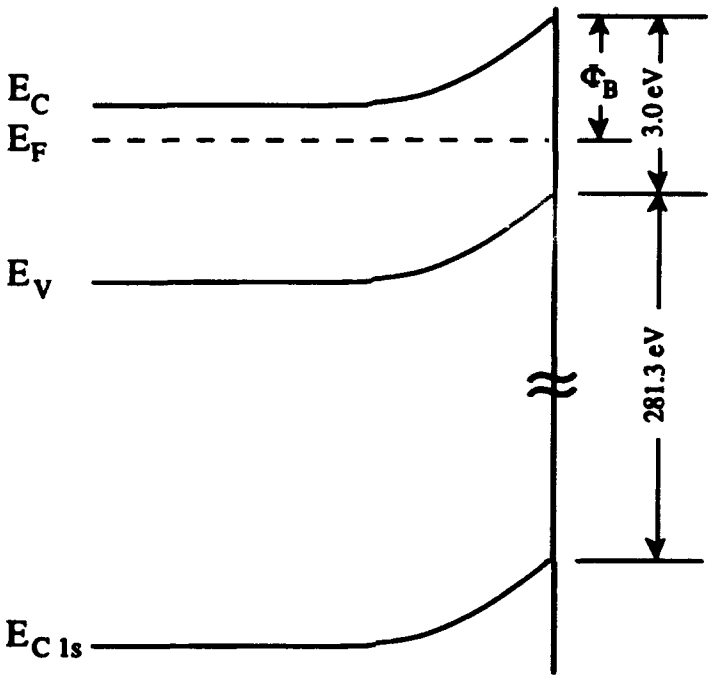

Figure 8. Energy band diagram of 6H-SiC showing the relationship between Φ_B and binding energies measured by XPS.

Referring to Fig. 8, the SBH can be determined by the following expression:

$$\Phi_B = \left[(E_{C1s} - E_V) + E_g\right] - E_{C1s}, \tag{6}$$

where E_{C1s} is the C 1s binding energy originating at the SiC surface, (E_{C1s} - E_V) is the C 1s to valence band maximum binding energy difference (constant for a given material), and E_g is the band gap. A value of E_{C1s} - E_V = 281.30 eV was obtained from the SiC surface prior to metal deposition by extrapolating the leading edge of the valence band spectra to zero intensity. This value agrees very well with the 281.26 ± 0.1 eV value determined by Waldrop *et al.* [12]. Substituting values into Eq. 6, the expression can be rewritten as

$$\Phi_B = 284.3 - E_{C1s}\ (\text{eV}). \tag{7}$$

Therefore, the amount of band bending at the SiC surface prior to metal deposition is determined by the position of the C 1s peak. After deposition of the metal, shifts in core levels are used to calculate the SBH.

A deconvolution procedure was used to separate effects due to changes in chemical bonding and changes in band bending. One or more peaks, which typically were 20–30% Gaussian and 70–80% Laurentzian, were fit to the core levels of interest. The peaks were located by the midpoints of their full widths at half maximum (FWHM), which were 0.78–0.80 eV. The Si-bound-to-C part of the Si 2p peak and the C-bound-to-Si part of the C 1s peak were used to determine band shifting before and after the Ti depositions.

Table I lists the binding energies of the Si 2p (Si-bound-to-C) and C 1s (C-bound-to-Si) peaks after depositing 0, 4, 8, and 12Å of Ti. The total band bending at the SiC surface before deposition of Ti was determined by subtracting the C 1s binding energy from 284.30 eV (see Eq. 7). These results indicated that the energy difference between the conduction band minimum and Fermi level at the surface was 0.40 ± 0.1 eV.

Table I. Binding energies of Si 2p and C 1s peaks peaks from SiC with various thicknesses of Ti. These binding energies have been corrected according to the Au $4f_{7/2}$ peak. Units are in electron-volts.

XPS peak	0 Å Ti	4 Å Ti	8 Å Ti	12 Å Ti
Si 2p	101.74	101.40	101.38	101.34
C 1s	283.90	283.62	283.56	283.52

Because these layers were so thin, it was important to make sure that complete coverage was achieved. Two-dimensional layer-by-layer growth, or Frank-van der Merwe growth, results in greater reduced intensities of the peaks originating from the substrate than three-dimensional island growth (a.k.a. Volmer-Weber growth). An expression for the reduced intensities of the substrate peaks for layer-by-layer growth is expressed by the following relationship [13, 14]:

$$I_{red} = (1-\Theta)\exp\left(\frac{-(n-1)m}{\lambda}\right) + \Theta\exp\left(\frac{-nm}{\lambda}\right), \quad (8)$$

where Θ equals the covered monolayer fraction, n is the number of monolayers, m is the thickness of one monolayer, and λ is the attenuation length of the emitted electrons. The attenuation length is relatively independent of the particular material but is a function of the energy of the electrons. For C 1s and Si 2p peaks, λ is equal to approximately 7 monolayers

[7]. Between integer numbers of monolayer coverage (e.g., n = 1, Θ = 1 to n = 2, Θ = 1), the reduced intensity decreases linearly with Θ. At integer numbers of monolayer coverage, where Θ = 1, Eq. 4.2-4 becomes

$$I_{red} = \exp\left(\frac{-nm}{\lambda}\right). \tag{9}$$

The reduced intensity (of either C 1s or Si 2p peaks) according to the layer-by-layer growth model is plotted vs. Ti thickness in Figure 9. The thickness of one monolayer, m, was approximated to be 1/2 c = 2.34 Å for Ti, which has an hcp structure with a=2.95 Å and c=4.68 Å. The C 1s and Si 2p reduced intensities calculated and normalized from the peak areas are also plotted vs. Ti thickness in Fig. 9. The data points follow the theoretical curve for two-dimensional growth very closely.

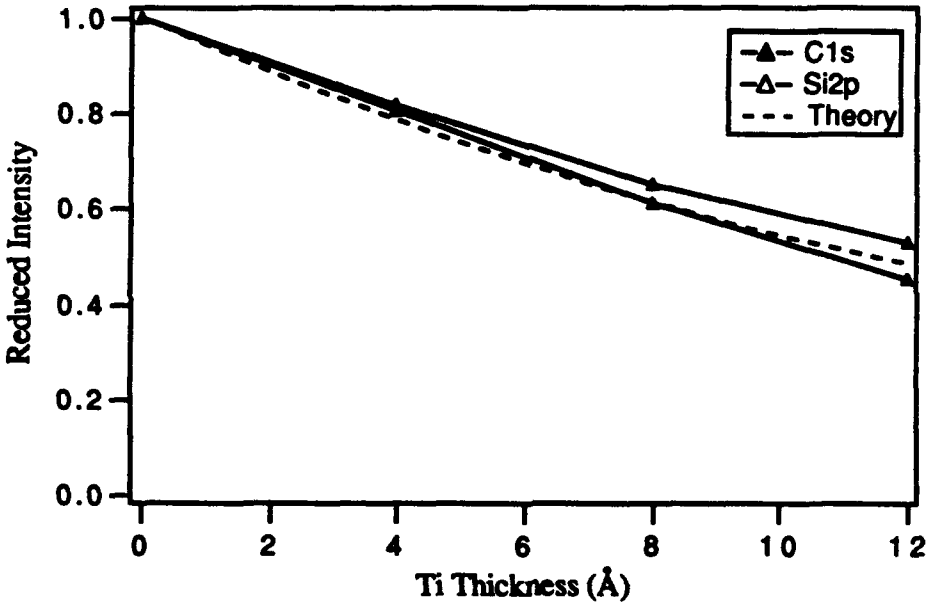

Figure 9. Plot of the reduced intensities of the C 1s and Si 2p peaks vs. Ti overlayer thickness as measured by the quartz deposition (film thickness) monitor. The theoretical curve represents layer-by-layer (Frank-van der Merwe) growth.

After depositing 4 Å of Ti, the Si 2p and C 1s binding energies (Table 1) were reduced by 0.34 and 0.28 eV, respectively, which corresponds to an increase in band bending. Most of the band bending occurred with the deposition of the first 4 Å of Ti. With 12 Å of Ti the total reduction in binding energies of the Si 2p and C 1s peaks were 0.40 and 0.38 eV, respectively. The difference in the binding energy shifts was within experimental error. The reduction in binding energies corresponded to an increase in the barrier height. Taking the average of the binding energy reductions and adding it to the initial amount of band bending gave a barrier height of 0.79 ± 0.1 eV.

The SBH's of Ti contacts on SiC calculated from I-V, C-V, and XPS measurements are summarized in Table II. The XPS analyses were performed only on as-deposited contacts, and C-V data was not obtained for samples annealed at 700°C for 40 min. However, of the data collected, the agreement is very good, within 0.15 eV, between the three measurement techniques.

Table II. Barrier heights of unannealed and annealed Ti contacts on SiC measured by I-V, C-V, and/or XPS.

anneal condition	$\Phi_B^{I\text{-}V}$ (eV)	$\Phi_B^{C\text{-}V}$ (eV)	Φ_B^{XPS} (eV)
unannealed	0.83	0.88	0.79
700°C / 40 min.	0.86	——	——
700°C / 60 min.	0.90	1.04	——

Interface Structure. The room temperature deposition of Ti on 6H-SiC (0001) resulted in epitaxial films. Both Ti (a = 2.95 Å, c = 4.68 Å) and 6H-SiC (a = 3.08 Å, c = 15.11 Å) have hexagonal crystal structures, corresponding to a -4% lattice mismatch between $(1\bar{1}00)_{Ti}$ and $(1\bar{1}00)_{SiC}$. The first indication of epitaxial growth was a 1×1 LEED pattern, similar to that of the SiC substrate, which was obtained from a deposited film of Ti (≈ 200 Å). Diffraction patterns of 6H-SiC and the Ti/6H-SiC interface are compared in Figure 10. Figure 10(a) shows a diffraction pattern of the 6H-SiC substrate along the zone axis $[1\bar{1}\bar{2}0]$, which is perpendicular to the [0001] direction. In Fig. 10(b) the diffraction pattern was obtained from an area which includes the interface of a cross-sectional Ti/SiC sample. The arrows mark spots from the Ti film. The other spots which are not present in (a) also originate from the Ti film. The fact that the Ti spots lie outside the SiC spots shows that the lattice parameter of the Ti film is smaller than that of the SiC substrate. The crystallographic relationships are $(0001)_{Ti} \parallel (0001)_{SiC}$ and $(\bar{1}\bar{1}00)_{Ti} \parallel (\bar{1}\bar{1}00)_{SiC}$.

The integrity of the interface structure is represented well by the HRTEM image shown in Figure 11. The top part of the figure shows a high resolution image of the Ti/SiC interface region. The enclosed area is magnified in the bottom part of the figure. The image shows a nearly perfect interface. The arrow at the interface shown in Fig. 11 marks a location which was initially thought to be a misfit dislocation but was later found to be a step at the SiC surface.

Also marked in the magnified image are the nearest plane spacings perpendicular to the interface. In Ti, which has a 2-layer periodicity, the nearest-neighbor planes are (0002) along the [0001] direction. The corresponding nearest-neighbor planes in 6H-SiC are (0006).

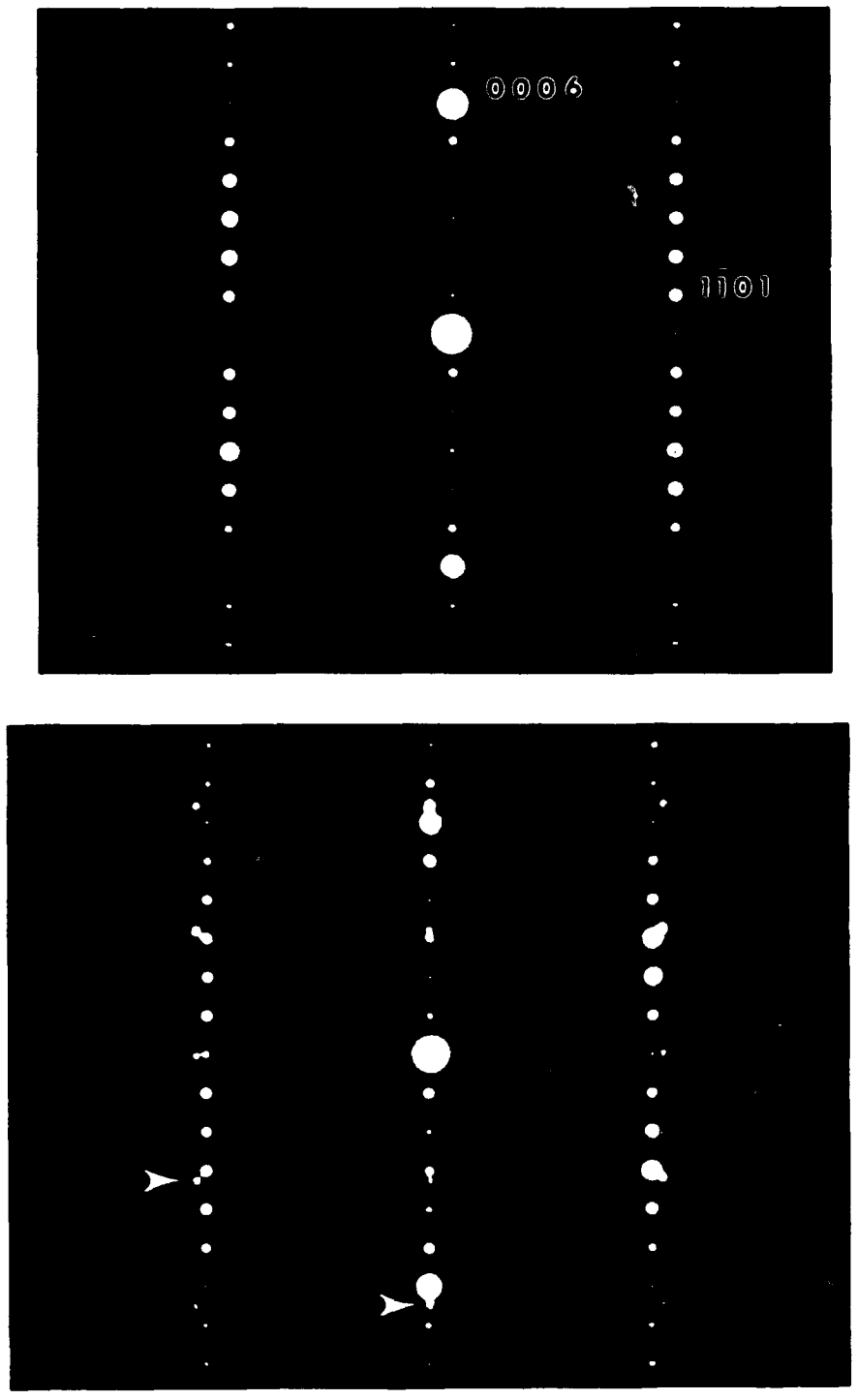

Figure 10. Selected area diffraction patterns of (a) 6H-SiC and (b) Ti/SiC interface in cross-sectional view. Two of the spots due to the Ti film are marked with arrows in (b). z = [11$\bar{2}$0].

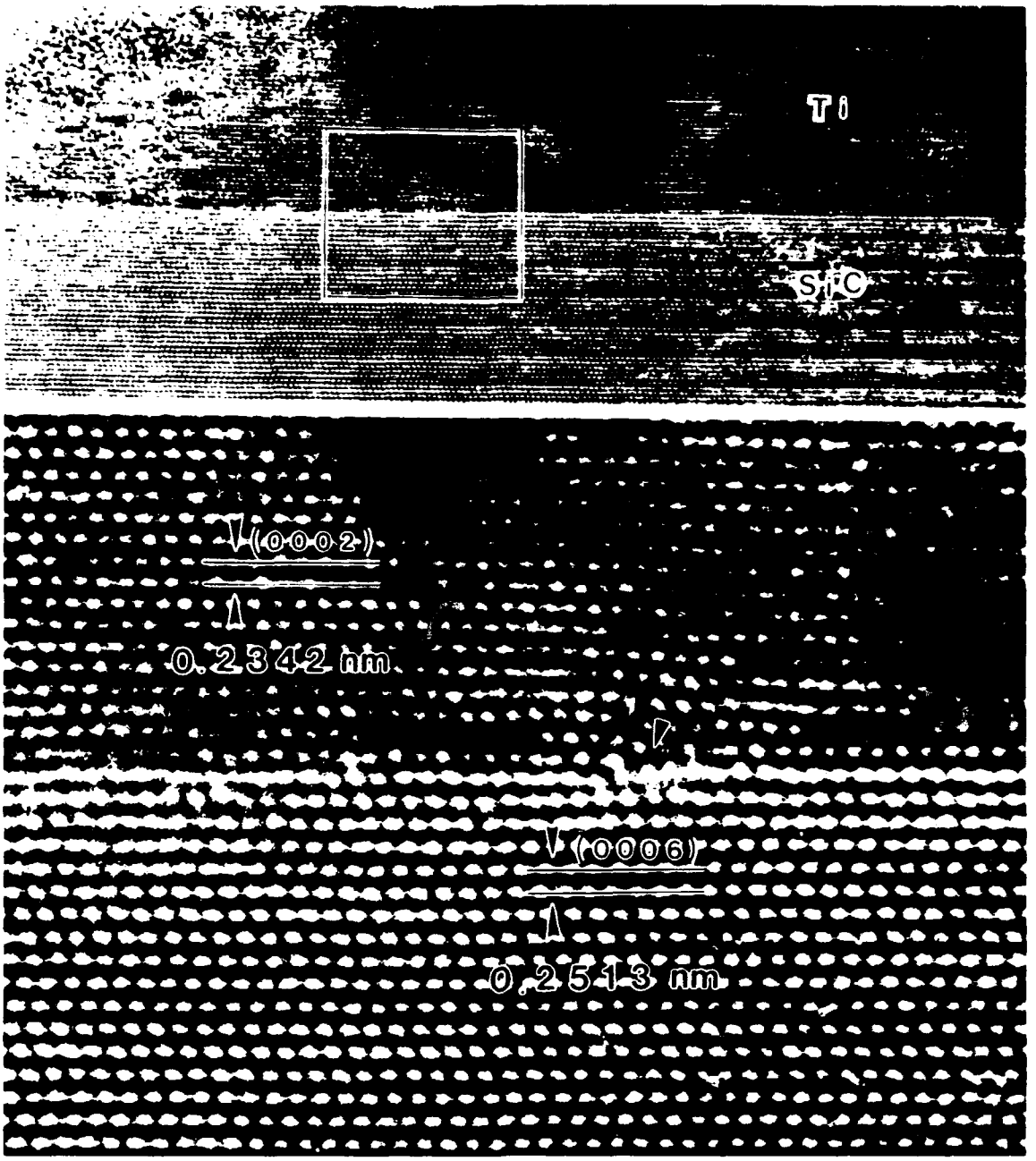

Figure 11. High resolution TEM image of as-deposited Ti/SiC in cross-section. The lower image is a magnification of the boxed-in region. The arrow at the interface marks the position of a misfit dislocation.

Interface Chemistry. After annealing at 700°C for 20 minutes, the interface reaction zone (R.Z.) consisted of a 2 to 3 nm thick, continuous layer of cubic (B1 (NaCl structure)) TiC_{1-x} in contact with the SiC and a layer of orthorhombic Ti_5Si_3 containing discrete TiC_{1-x} particles at the Ti side of the interface (Fig. 12). The total width of the R.Z. was 10 to 15 nm. The size of the TiC_{1-x} particles was 5 ± 2 nm. The major product phase, Ti_5Si_3, was a continuous layer which contained low angle boundaries.

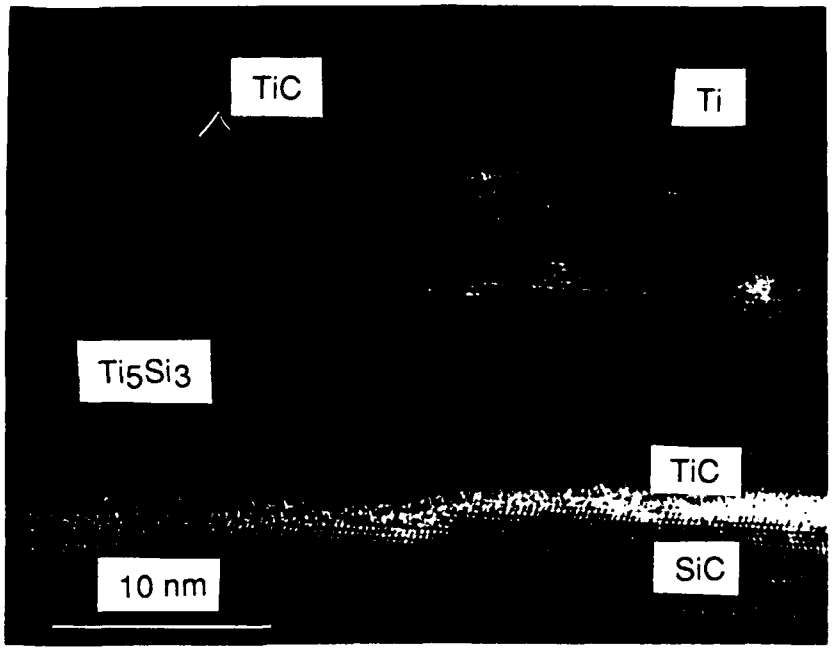

Figure 12. High resolution TEM micrograph of Ti/SiC interface after annealing for 20 min. at 700°C in UHV.

The width of the reaction zone did not change after annealing for 60 minutes (Fig. 13). However, the TiC_{1-x} particles disappeared at the interface with Ti. The position of the layers

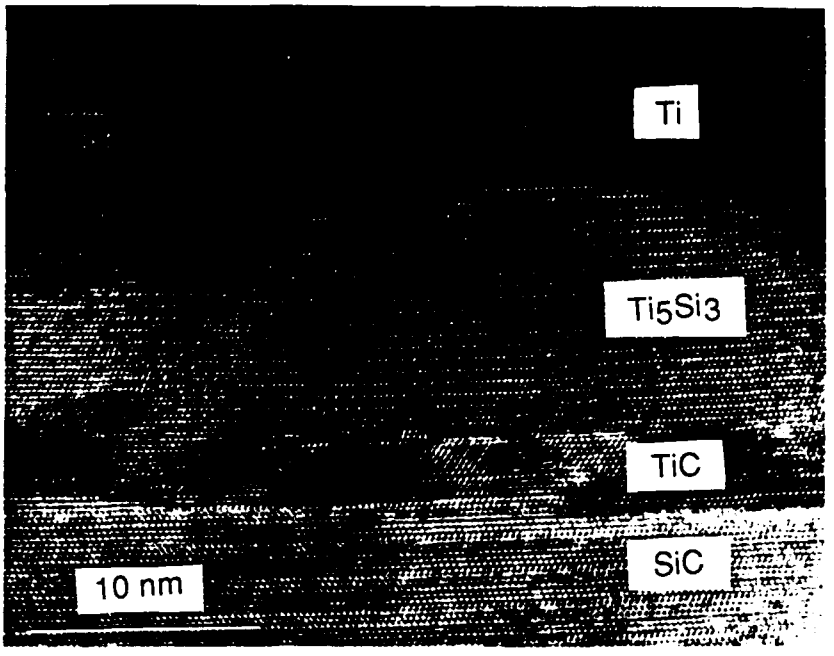

Figure 13. High resolution TEM micrograph of Ti/SiC interface after annealing for 60 min. at 700°C in UHV.

comprising the interface was SiC / TiC_{1-x} / Ti_5Si_3 / Ti. The lattice parameter of TiC_{1-x} varied by approximately 2% along the SiC interface. The crystallographic relationships are summarized by the following:

$$(0001)_{SiC} \parallel (11\bar{1})_{TiC_{1-x}} \parallel (0001)_{Ti_5Si_3} \parallel (0001)_{Ti}$$
$$[11\bar{2}0]_{SiC} \parallel [011]_{TiC_{1-x}} \parallel [45\bar{1}0]_{Ti_5Si_3} \parallel [11\bar{2}0]_{Ti}.$$

Concentration profiles obtained by EDS perpendicular to the interface before annealing and for anneals of 20 min. and 60 min are shown in Figure 14. The resolution is approximately 5 nm as determined by the profile of the as-deposited Ti/SiC interface. After annealing for 20 min., the C concentration showed a high level near the SiC interface in addition to a peak near the interface with Ti. A peak in the Si concentration occurred in the reaction zone (R.Z.) closer to the the SiC. This type of profile occurred because of the faster diffusivity of C than Si in all the reaction products. During the 60 min. anneal, the C near the Ti interface diffused into the Ti, while more of the Si diffused through the reaction zone. These profiles correspond to the reaction phases shown in Figs. 12 and 13.

The α-Ti hcp phase is stable up to 882°C [15]; therefore, there should be no polymorphic transformation of the Ti phase. At the annealing temperature of 700°C, TiC_{1-x} is the only binary phase which exists between the two elements. At this temperature, TiC_{1-x} covers a range of stoichiometries from approximately 40.5 to 48.5 atomic percent C, while approximately 1.0% C and < 0.5% Si are soluble in α-Ti. There are five titanium silicides at this temperature: Ti_3Si, Ti_5Si_3, Ti_5Si_4, TiSi, and $TiSi_2$.

The free energies of formation of the carbide and silicides with Ti at 700°C are listed in Table III. TiC has by far the lowest free energy of formation at this temperature, while TiSi, Ti_5Si_4, and Ti_5Si_3 have free energies of formation within 10.0 kJ/mol of each other.

Table III. Free energies of formation of binary Ti compounds with Si and C at 700°C.

Compound	ΔG (kJ/mol)	Reference
Ti_3Si	-61.3	[15]
Ti_5Si_3	-85.6	[15]
Ti_5Si_4	-87.7	[15]
TiSi	-95.1	[15]
$TiSi_2$	-77.7	[15]
TiC	-172.6	[16]

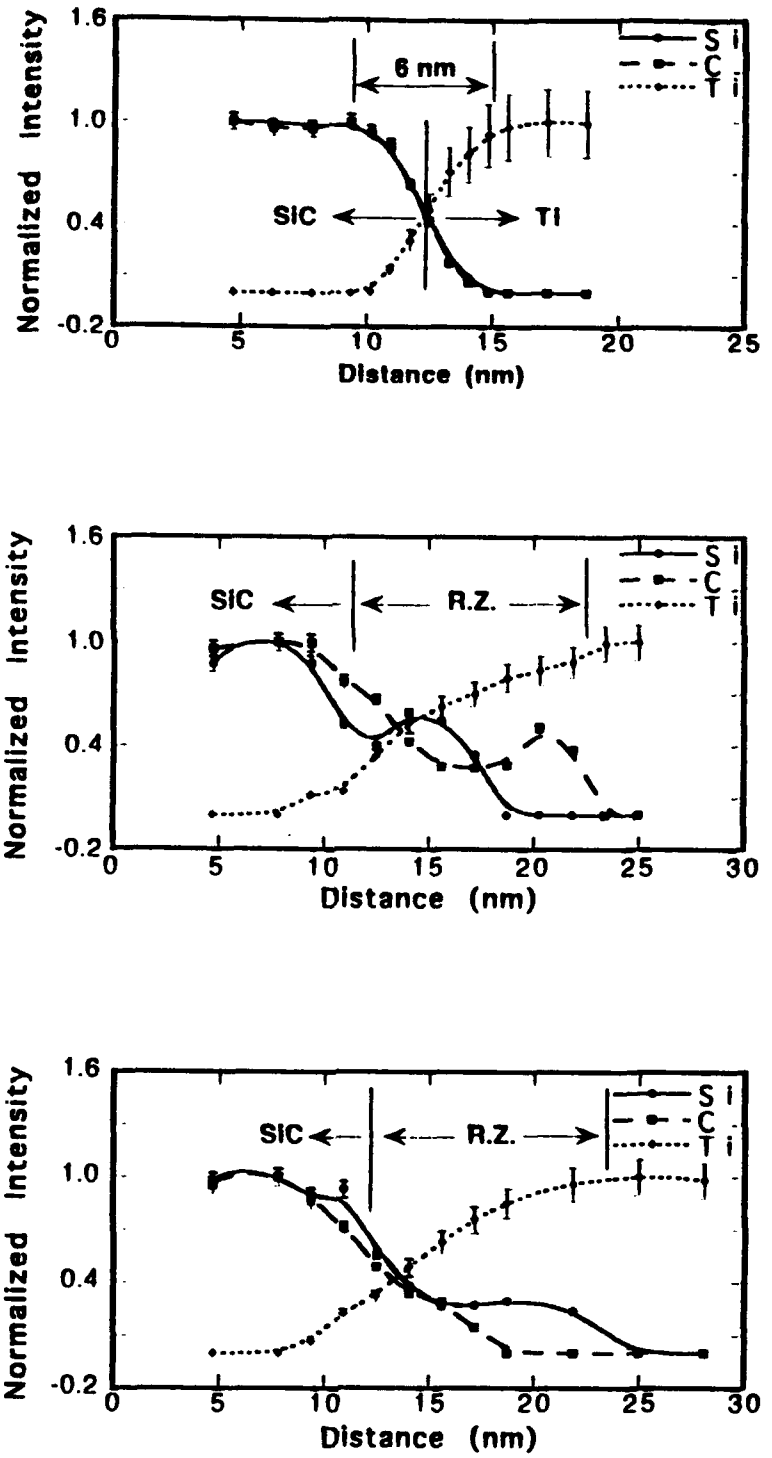

Figure 14. Concentration profiles of Si, C, and Ti perpendicular to the Ti/SiC interface determined by parallel electron energy loss spectroscopy (PEELS) after annealing at 700°C for (a) 20 min. and (b) 60 min.

There seems to be no simple way of predicting the total diffusion path in a material system having three or more components and which is in the process of attaining thermodynamic equilibrium, e.g., Ti and SiC chemically bonded at an interface and heated to

the extent that chemical interdiffusion occurs. Knowledge of all the thermodynamic data is, in general, not sufficient to predict which product phases will form. Thermodynamic data (i.e. temperature, pressure, and free energies) can yield the equilibrium phase fields; however, the diffusion path is controlled by the diffusion coefficients of each component in the pertinent phases. It is the ratio of the diffusivities which determines the interface compositions, and accordingly the diffusion path [17]. Therefore, one must be wary of predictions made for multicomponent systems when only thermodynamic constraints are used. There has been evidence in many metal/SiC systems that the reactions were limited by the dissociation of SiC, resulting in metal-rich silicides.

There have been several extensive studies of the Ti-Si-C system at high temperatures. At temperatures between 570°C and 1200°C and at low or atmospheric pressures, the product phases in Ti/SiC diffusion couples were reported to be TiC [18, 19], Ti_5Si_3 [20], or both TiC_{1-x} and Ti_5Si_3 [21-24]. At high pressures (10 to 20 kbars) and high temperatures (1200°C to 1500°C) $Ti_3SiC_{(1.78-2.00)}$ was identified along with TiC_{1-x} and Ti_5Si_3 [25]. At the high end of this pressure range Ti_3Si formed, which exhibited a high solubility for carbon (up to 9 at. %).

Backhaus-Ricoult [22, 23] studied diffusion couples between Ti and polycrystalline SiC at 1200°C. By measuring the concentration profiles of each of the constituents and plotting them on the Ti-Si-C Gibbs phase triangle, the diffusion path was determined. It was stated that because the diffusion of C in Ti is ≈10 times faster than Si in Ti, the reaction runs from pure Ti to the Si-rich corner of the Ti phase field, which is is connected to the Ti_5Si_3 phase field. The concentration of the slower diffusing Si quickly increases near the interface and reaches its solubility limit, at which point Ti_5Si_3 forms. The reaction path then passes through the phase field containing Ti_5Si_3, TiC_{1-x}, and Ti. Carbon reacts with Ti to form TiC within the Ti_5Si_3 phase. The morphology of the product layer showed the formation of TiC_{1-x} particles throughout a matrix of Ti_5Si_3, where the TiC particles contained more C closer to the SiC interface.

It is worthwhile to make some comparisons between our results and those just described. The Ti/SiC samples in the present research were annealed at 700°C; however, the same phases were formed in the reaction as those found at 1200°C. The diffusion paths are apparently very similar if not the same. The faster diffusivity of C in Ti would explain the formation of the TiC particles at the interface with Ti early in the annealing stage. An important difference is that a continuous TiC layer formed along the interface with SiC. It is believed that Backhaus-Ricoult [22, 23] could not have seen this initial TiC layer without the use of high resolution TEM. It is also possible that the TiC layer formed to minimize interface strain between the phases in the reaction zone and the monocrystalline 6H-SiC (0001) used in the present study. A large lattice misfit strain (~8.5%) exists between

$(2130)_{Ti_5Si_3}$ and $(\bar{1}\bar{1}00)_{6H\text{-}SiC}$, which were both normal to the $(0001)_{SiC}$ interface plane and parallel to eachother. The resulting morphological sequence, which was described above, is more favorable in terms of strain. Between $(\bar{1}\bar{1}1)_{TiC}$ and $(1\bar{1}02)_{SiC}$ there is only a 0.5% mismatch, while that between $(111)_{TiC}$ and $(21\bar{3}0)_{Ti_5Si_3}$ is 2.5%.

Chemical bonding at the interface was studied by XPS after depositing a series of thin Ti films. Figure 15 shows the C 1s and Si 2p peaks after depositing 4, 8, and 12 Å Ti. Each of these peaks has been deconvoluted into a major and a minor peak.

After 4 Å of Ti was deposited, the C 1s peak was composed of a major peak at 283.62 eV and a minor peak at 282.04 eV. With thicker films of Ti, the minor peak grew; after 12 Å of Ti both peaks shifted to slightly lower binding energies of 283.52 eV and 281.94 eV, respectively. The major peak originates from C-bound-to-Si in SiC, and the minor peak is attributed to C-bound-to-Ti [26]. The increasing contribution of the minor peak at the greater film thicknesses is a result of the corresponding reduction in sensitivity to the SiC. Titanium-carbon bonding is expected due to the highly negative free energy of formation of TiC.

Titanium silicide bonding was not detected. Because titanium has a lower electronegativity (1.54) than carbon (2.55), Si-Ti bonding should result in a peak at the low binding energy side of the Si 2p (Si-bound-to-C) peak. Instead, a minor peak at slightly higher binding energy was detected. After 4 Å Ti was deposited, the major and minor peaks were located at 101.40 eV and 102.56 eV, respectively. The minor peak is probably due to SiO_x, since the same binding energy difference existed prior to Ti deposition. Si 2p binding energies reported in the literature are ≈103.7 eV for SiO_2 [27]and 102.7 eV for SiO [5].

The combination of XPS and TEM analyses shows that interfacial TiC formation begins with an initial two-dimensional coverage of Ti at room temperature and is enhanced after annealing at 700°C. On the other hand, there seems to be some O which remains at the interface bonded to Si. The amount of oxygen does not appear to be sufficiently high to interfere with creating a high quality interface, as indicated by high resolution TEM.

D. Conclusions

A comprehensive study of the electrical properties, microstructure, and chemistry of both as-deposited and 700°C annealed thin film Ti/6H-SiC (0001) interfaces was performed with specific regard to the application of contacts in semiconductor devices.

As-received, thermally oxidized, n-type 6H-SiC (0001) substrates were simultaneously cleaned and etched in either an ethanol / hydrofluoric acid / water (10:1:1) or a 10% hydrofluoric acid solution followed by a 15 min. thermal desorption at 700°C in UHV. This procedure resulted in 1x1 unreconstructed surfaces which contained submonolayer residual O and trace amounts of F. X-ray photoelectron spectroscopy analyses revealed that the energy bands bent upwards at the surface. This result indicates that surface states were present,

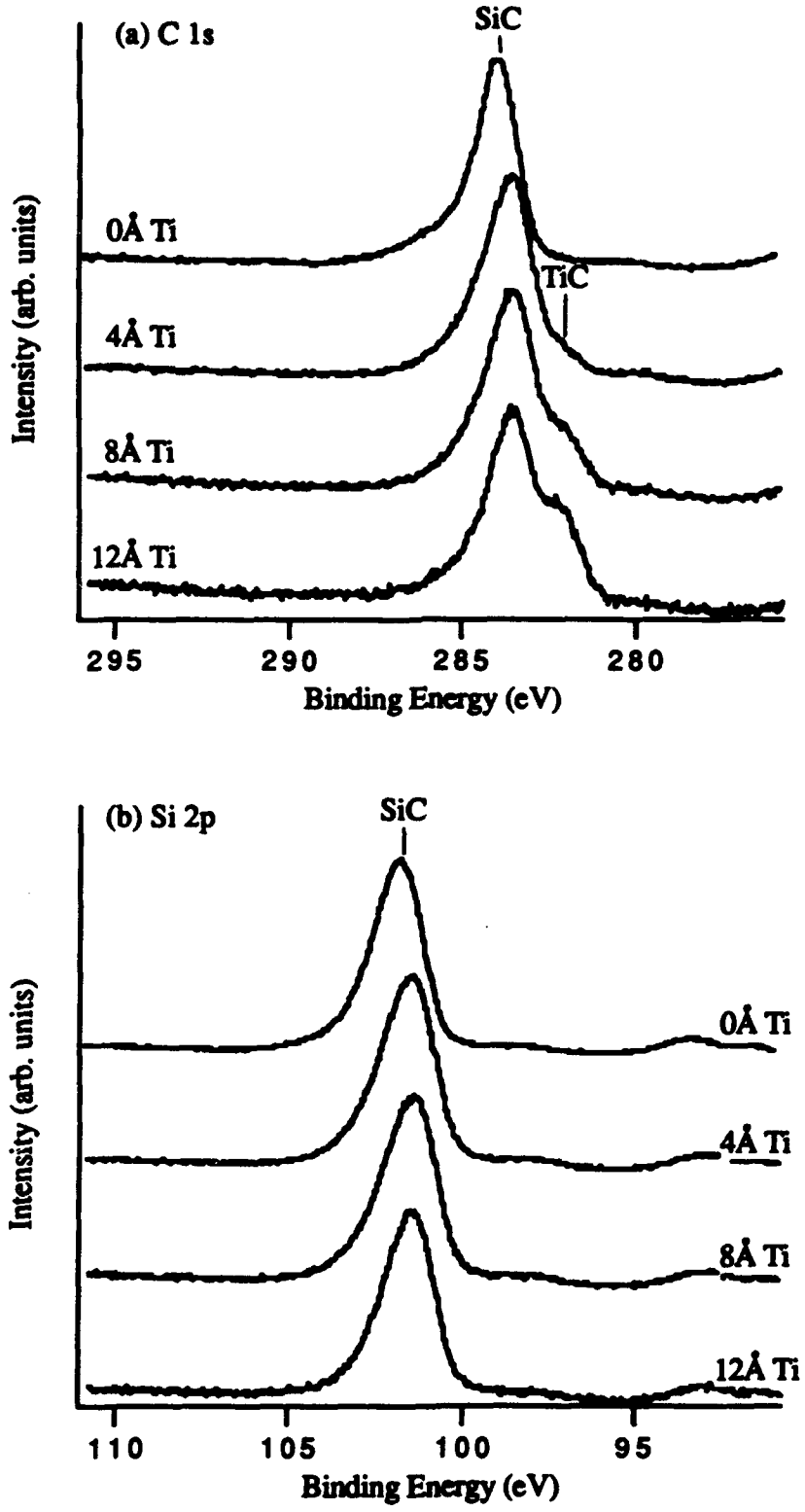

Figure 15. XPS C 1s and Si 2p peaks from SiC after 4, 8, and 12 Å Ti.

which acted as acceptors and which are expected to prohibit an exact correlation between the Schottky barrier heights and metal work functions as predicted by the Schottky-Mott limit for ideal metal-semiconductor contacts.

The deposition of Ti onto these chemically-treated, unheated SiC substrates resulted in epitaxial contacts, which exhibited rectifying behavior, low ideality factors ($n < 1.09$), and typical leakage currents of 5×10^{-7} A/cm^2 at -10V. The SBH's calculated from I-V, C-V, and XPS measurements (0.79–0.88 eV) were somewhat lower than that predicted by the Schottky-Mott limit (1.03 eV). This result may be associated with surface states in the SiC substrates. On the other hand, other metal contacts would need to be examined to understand the relationship of the surface states to the resulting Schottky barrier heights.

The SBH's and electrical properties do not show substantial changes after annealing at 700°C for up to 60 min., except after an initial 20 min. anneal. However, interfacial chemical reactions resulted in the formation of Ti_5Si_3 and TiC_{1-x}, which is in agreement with several previous studies. The fact that the formation of Ti_5Si_3 and TiC, which are low work function metals [28, 29], did not result in a reduction of the SBH suggests that energy states were also present at the newly-created interface between TiC and SiC.

E. Future Research Plans/Goals

The current technology of SiC devices is driving the need for ohmic contacts to p-type SiC which have low contact resistivities at both room and elevated temperatures. Aluminum alloys are currently used because the Al degeneratively dopes the surface of the SiC, which reduces the contact resistance. However, these contacts cause problems at elevated temperatures due to melting and extensive diffusion.

Our plan is to investigate other materials which should be more stable at elevated temperatures. The issues being considered for both choosing the material(s) and conducting the experiments are work function differences, lattice mismatch, thermal properties, and doping profiles/concentrations. After depositing the chosen material(s), the I-V characteristics and the contact reisistivities will be measured at room and elevated temperatures.

F. References

1. W. O. Saxton, T. J. Pitt, and M. Horner, Ultramicroscopy, 4 (1979) 343.
2. *Handbook of X-ray Photoelectron Spectroscopy* , edited by C.D. Wagner, W.M. Riggs, L. E. Davis, and J. F. Moulder (Perkin-Elmer Corp., Eden Prairie, MN, 1979).
3. J. R. Waldrop and R.W. Grant, Appl. Phys. Lett., **62** (1993) 2685.
4. D. B. Fenner, D. K. Biegelsen, and R. D. Bringans, J. Appl. Phys., **66** (1989) 419.
5. J. A. Taylor, G. M. Lancaster, A. Ignatiev, and J. W. Rabalais, J. Chem. Phys., **68** (1978) 1776.
6. K. L. Smith and K. M. Black, J. Vac. Sci. Technol. A, **2** (1984) 744.
7. *Auger and X-ray Photoelectron Spectroscopy* 2nd ed. Practical Surface Analysis, Vol. 1 edited by D. Briggs and M. P. Seah (John Wiley & Sons, New York, 1990).

8. R. Kaplan, Surface Science, **215** (1989) 111.
9. R. T. Tung, Phys. Rev. B, **45** (1992) 13509.
10. J. W. Palmour (Cree Research, Inc., Research Triangle Park, North Carolina, USA, 1992) private communication.
11. S. M. Sze, *Physics of Semiconductor Devices* 2nd ed. (John Wiley & Sons, Inc., New York, 1981).
12. J. R. Waldrop, R. W. Grant, Y. C. Wang, and R. F. Davis, J. Appl. Phys., **72**, 4757 (1992).
13. L. C. Feldman and J. W. Mayer, *Fundamentals of Surface and Thin Film Analysis* (North-Holland, New York, 1986).
14. Z. Sitar, L. L. S. Smith, and R. F. Davis, Submitted to J. Cryst. Growth.
15. *Phase Diagrams of Binary Titanium Alloys*, Monograph Series on Alloy Phase Diagrams, edited by J.L. Murray (ASM International, Metals Park, Ohio, 1987).
16. *JANAF Thermochemical Tables*, Journal of Physical and Chemical Reference Data, Vol. 14, edited by M. W. Chase Jr., C. A. Davies, J. R. Downey Jr., D. J. Frurip, R. A. McDonald, and N. A. Syverud (The American Chemical Society and The National Institute of Physics for the National Bureau of Standards, Midland, MI, 1985).
17. G. R. Purdy, D. H. Weidel, and J. S. Kirkaldy, Trans. Met. Soc., **230** (1964) 1025.
18. M. B. Chamberlain, Thin Solid Films, **72** (1980) 305.
19. J. J. Bellina Jr. and M. V. Zeller, Mat. Res. Soc. Symp. Proc., **97** (1987) 265.
20. M. Nathan and J. S. Ahearn, Materials Science and Engineering, **A126** (1990) 225.
21. C. G. Rhodes and R. A. Spruling in *Recent Advances in Composites in the United States and Japan*, edited by J. R. Vinson and M. Taya, (American Society for Testing and Materials: Philadelphia, 1985).
22. M. Backhaus-Ricoult, Ber. Bunsenges. Phys. Chem., **93** (1989) 1277.
23. M. Backhaus-Ricoult in *Metal-Ceramic Interfaces*, edited by M. Ruhle, *et al.*, (Pergamon Press, New York, 1990).
24. I. Gotman, E. Y. Gutmanas, and P. Mogilevsky, J. Mater. Res., **8** (1993) 2725.
25. S. Sambasivan and W. T. Petuskey, J. Mater. Res., **7** (1992) 1473.
26. L. Ramqvist, K. Hamrin, G. Johansson, A. Fahlman, and C. Nordling, J. Phys. Chem. Solids, **30** (1969) 1835.
27. T. L. Barr, Appl. Surf. Sci., **15** (1983) 1.
28. G. V. Samsonov, L. N. Okhremchuk, N. F. Podgrushko, I. A. Podchernyaeva, and V.S. Fomenko, Inorganic Materials, **12** (1976) 720.
29. K. Senzaki and Y. Kumashiro, Bull. Electrotech. Lab. Jpn., **41** (1977) 593.

VI. Distribution List

	Number of Copies
Dr. Yoon Soo Park Office of Naval Research Applied Research Division, Code 1261 800 N. Quincy Street Arlington, VA 22217-5660	3
Administrative Contracting Officer Office of Naval Research Resident Representative The Ohio State Univ. Research Ctr. 1960 Kenny Road Columbus, OH 43210-1063	1
Director Naval Research Laboratory ATTN: Code 2627 Washington, DC 20375	1
Defense Technical Information Center Bldg. 5, Cameron Station Alexandria, VA 22304-6145	2